ABSTRACT

MCENTEE, CATHERINE MARIE. Distribution Volt-Var Control through Coordination of Smart Solar Inverters and Utility Control Devices Considering Limited Visibility and Legacy Devices (Under the direction of Dr. Ning Lu).

This dissertation first presents a centralized volt-var control (CVVC) algorithm to coordinate customer-owned controllable loads and smart solar inverters with utility-owned voltage regulators and capacitors to meet voltage control objectives. The optimization problem is formulated as a mixed-integer nonlinear programming (MINLP) problem. A voltage sensitivity matrix (VSM) is used to linearize the effect of control actions on the voltage at customer nodes when solving the MINLP. The VSM is recalculated at each time step to improve the computational accuracy. Both discrete switching actions of the capacitor and VRs and the continuous adjustment of real and reactive power from load and smart inverters are considered in the MINLP volt-var problem formulation. The objective function minimizes the cost of all control actions and the magnitude of voltage fluctuations from the previous time period. Constraints ensure that the voltage at each node is maintained within ANSI limits and the feeder power factor is controlled within the desired range. The CVVC is extended to coordinate with transmission for integrated control, and the coordinative CVVC is tested on a networked hardware-in-the-loop real-time testbed.

Then, to address the practical concerns of visibility and computational speed, a regression-based method for estimating voltages and voltage sensitivities for volt-var control on distribution circuits with limited data is presented. The estimator uses power flow results for representative load and PV output scenarios as training data. Using linear regressions on power flow results, the voltages at critical nodes are calculated online based on power measurements at the feeder head and at each PV plant. The voltage sensitivity to changes in reactive power

injection by each PV plant is also found online using regressions trained offline on power flow results. The estimator thus provides the estimated critical voltages and their sensitivities to each possible control action. The estimator is tested in conjunction with a volt-var optimization on a real, unbalanced rural distribution feeder. Results show that the estimator can estimate voltages and sensitivities with adequate accuracy for successful centralized volt-var control.

Distribution Volt-Var Control through Coordination of Smart Solar Inverters and Utility Control Devices Considering Limited Visibility and Legacy Devices

by
Catherine McEntee

A dissertation submitted to the Graduate Faculty of
North Carolina State University
in partial fulfillment of the
requirements for the degree of
Doctor of Philosophy

Electrical Engineering

Raleigh, North Carolina
2020

APPROVED BY:

_____	_____
Dr. Ning Lu Committee Chair	Dr. David Lubkeman
_____	_____
Dr. Mesut Baran	Dr. Timothy Menzies

DEDICATION

To my friends, family and mentors who made this possible.

BIOGRAPHY

Catie McEntee received her Bachelors in Electrical Engineering in 2015 and her Masters in Electric Power Systems Engineering in 2016, both from NC State University. She is currently pursuing her Ph.D. in Electrical Engineering at NC State University. Her research interests include distribution system planning and operations with renewables and energy storage.

ACKNOWLEDGMENTS

This accomplishment would not be possible without the support of my friends and family, the guidance of my professors and advisors, and considerable teamwork from my lab mates and colleagues. My advisor, Dr. Ning Lu, introduced me to the world of research. She entrusted me with innovative projects and challenged me to continuously improve the quality of my work. Along with Dr. Lu, my committee members, Dr. David Lubkeman and Dr. Mesut Baran taught me nearly everything I know about power systems, and have always provided valuable feedback to extend and improve my work. I also thank Dr. Tim Menzies for his great willingness to help me and for offering a new perspective when I needed it most.

A huge thanks goes to David Mulcahy for introducing me to Python and other essential tools for surviving graduate school. Thanks also to Landon Mackey for convincing me to go to graduate school, Inalvis Alvarez and Valentin Rigoni for inspiring me and believing in me, Kelina Farnham for keeping me sane during the COVID-19 stay-at-home order, Elyse Mark for getting me through high school and Paul Hicks for being there for me through college. To you and many others who helped along the way: I couldn't have done this without your love and support.

My lab mates and colleagues deserve great appreciation for their contributions to this work: Xiangqi Zhu provided a jumping-off point for this dissertation, and David Mulcahy and Jiyu Wang were instrumental in helping to develop the initial implementation. Fuhong Xie and Minzhi Zhang made real-time testing possible. Xinda Ke, Renke Huang, Mallik Vallem, Malini Ghosal, and Nader Samaan at Pacific Northwest National Lab provided excellent collaboration on the transmission side of the CReST-VCT. Ming Liang, Asmaa Alrushoud and Ahmed

Abdelsamad provided have much appreciated feedback and moral support. I have been lucky to work alongside you all.

Finally, a special thanks goes to my parents Dave and Lisa McEntee, who have always believed in me and guided me toward the right path, and my husband Peter, who supports me in everything I do.

TABLE OF CONTENTS

LIST OF TABLES viii
LIST OF FIGURES ix
Chapter 1: Introduction 1
Introduction 1
Traditional Control Schemes 1
Growth of PV 2
PV impacts on utility/grid operations 2
Reverse power flow 2
PV Variability 3
Potential for PV to improve grid operations 3
Increasing PV hosting capacity 4
Centralized Volt-var Control 4
Chapter 2: VSM-Based DER Dispatch MINLP for Volt-Var Control in Unbalanced Power Distribution Systems 6
Background and Literature Review 6
MINLP-based CVVC Algorithm 9
Voltage Sensitivity Matrix 9
Mixed-Integer Nonlinear Program 10
Resource Cost Functions 13
Software Simulation Setup 14
Software Simulation Results 17
Accuracy of the VSM-based Voltage Calculation 17
Voltage Regulation 18
Computational speed 22
Real-Time Simulation Setup 23
The Configuration of the HIL Testbed 24
Real-time Simulation Results 28
Discussion 29
Chapter 3: Chapter 3: Coordinated Real-Time Sub-Transmission Volt-Var Control Tool (CREST-VCT) 31
Distribution Optimization Formulation 33
Real-time Test Setup 33
Real-time Test Results 35

Discussion and Future Work 36
Chapter 4: Chapter 4: A Regression-Based Voltage Estimation Method for Distribution Volt-Var Control with Limited Data 37
Introduction 37
Method 40
Representative Scenario Selection 41
Training Data Preparation 43
Critical Nodes Selection 44
Voltage Estimator and Voltage Sensitivity Estimator 45
Online Operation 47
Voltage Estimation 48
Voltage Estimation Correction 48
Command Implementation 49
Optimization Formulation 50
Simulation Results 52
Test Feeders and Data Sets 52
Case Setup 53
Efficacy of Representative Scenario Selection 54
Efficacy of Voltage Measurement Correction 55
Overall Performance Comparison 56
Impact of Voltage Estimation and Use of Critical Nodes 57
Impact of VR set points 57
Impact of voltage correction 57
Impact of Voltage Regulator Dead Band Settings 57
Comparison between Case A and Case D 58
Speed Comparison 60
Conclusion 61
Chapter 5: Summary and Future Work 63

LIST OF TABLES

Table 2.1. Optimization Parameters Used in Case Study 14

Table 2.2. Overall number or quantity of each control action and their costs for the base case and optimal case. 22

Table 2.3. Summary of Simulation Results for Different Margins 29

Table 4.1. Simulation Case Setup 53

Table 4.2. Rural Circuit Results Summary 56

Table 4.3. Summary of VR Bandwidth Impacts on the Rural Circuit in Winter 58

LIST OF FIGURES

Figure 2-1. Topology of a rural distribution feeder in North Carolina with 100% residential PV penetration (a) and 100% utility-scale PV penetration (b).....15

Figure 2-2. PV and net load for one winter week with 100% residential (a) and utility-scale (b) PV.....16

Figure 2-3. Error between nodal voltages calculated using VSM and power flow for the Residential PV case.....18

Figure 2-4. Error between nodal voltages calculated using VSM and power flow for the utility-scale PV case.....18

Figure 2-5. Range, middle 50% and median node voltages at each time step 19

Figure 2-6. Range, middle 50% and median node voltages at each time step 19

Figure 2-7. Optimal control actions for one week with residential (a) and utility-scale (b) PV.....20

Figure 2-8. Power factor at the substation with optimal control for the residential (a) and utility-scale (b) PV cases.....21

Figure 2-9. Boxplots showing the median (line), 25^{th} and 75^{th} percentiles (box) and range (whiskers) for time to calculate the VSM, time to solve the MINLP, and the total run time for each time step for the residential (a) and utility-scale (b) PV cases. 23

Figure 2-10. Architecture of the asynchronous HIL co-simulation platform. 24

Figure 2-11. Control timeline for two control intervals. 27

Figure 2-12. Nodal voltage profiles: (a) no-control baseline case and (b) controlled case with perfect communication. 28

Figure 2-13. Phase *a* voltage at Node 50 when using different voltage control margins.....29

Figure 3-1. CREST-VCT Operational Framework 31

Figure 3-2. CREST-VCT Operational Timeline 32

Figure 3-3. Networked HIL Testbed Setup 34

Figure 3-4. Networked HIL Testbed Communication Links.....34

Figure 3-5. Reactive power adjustment fulfillment.....35

Figure 3-6. Distribution Feeder Node Voltages with CREST-VCT.....36

Figure 4-1. Flowchart of the offline training and online operation processes 41

Figure 4-2. Selection of typical operation scenarios 42

Figure 4-3. (a) Minimum, maximum, and median load centers for one load/PV block and (b) resulting voltage profiles 43

Figure 4-4. Voltage profile with critical nodes 45

Figure 4-5. δQ variation with respect to other measurements 46

Figure 4-6. δQ with curve fit and residuals 47

Figure 4-7. Voltage error and correction factor, εr, for nodes downstream of two VRs for 3 different scenarios 49

Figure 4-8. Test feeder map with PV and VR locations 52

Figure 4-9. Voltage estimation error with (a) random and guided selection and (b) with and without voltage correction 55

Figure 4-10. Test Feeder with Critical Node Locations 55

Figure 4-11. 10-minute average voltage results on the rural curcuit in winter 59

Figure 4-12. Reactive power injections by each PV plant on the rural circuit in winter 59

Figure 4-13. Tap positions and number of tap changes for each VR on the rural circuit in winter 60

Figure 4-14. Computational speed comparison Boxplot 61

Chapter 1: **Introduction**

Introduction

Volt-var control has always been an essential function for distribution operations. In recent decades, volt-var control has been complicated by the addition of distribution-connected solar photovoltaic (PV) generating facilities. This dissertation proposes a novel method for central coordination of PV smart inverters with traditional utility voltage control equipment to improve voltage control in the presence of high PV penetration.

Traditional Control Schemes

The purpose of volt-var control is to maintain service voltages and power factors within defined limits to avoid damaging utility and customer equipment. Voltage limits are defined in ANSI standard C84.1 as within 95% and 105% of nominal [1]. Volt-var control also ensures efficiency of electricity delivery by reducing unnecessary reactive power flow, which increases losses, and enabling utility and customer equipment to operate within its rated (most efficient) voltage range.

Traditional volt-var control schemes rely on fixed and switched capacitors and voltage regulators (VRs). Capacitors supply reactive power close to the customer devices and distribution lines that absorb it in order to reduce reactive power flow throughout the circuit. Capacitors can reduce losses due to excess reactive power flow and increase voltages by reducing the component of voltage drop associated with reactive power flow [2]. Voltage regulating transformers (VRs) are employed within substations and further downstream on distribution circuits to buck or boost voltages as needed to maintain ANSI limits. In some cases, utilities opt to control voltages within a tighter band than prescribed by the ANSI standard in

order to reduce demand, as in conservation voltage reduction (CVR) or distribution-side demand reduction (DSDR).

Growth of PV

Solar photovoltaic generation (PV) has proliferated over the last several decades and will likely continue to grow as coal plants retire, as the cost of solar modules and associated equipment and labor continues to drop, and as public opinion shifts ever more toward clean, renewable energy. PV penetration in North Carolina has come largely in the form of utility-scale solar plants with 1 to 5 MW of capacity [3]. A single rural circuit in North Carolina can host one or a few multi-MW PV plants. In other areas, for example California, PV has mainly been implemented both in utility-scale plants and in smaller residential installations of less than 10 kW [4]. In these cases, a single feeder could host hundreds of residential PV systems.

PV impacts on utility/grid operations

While PV technology has been in use for decades, the ever-growing amount of distribution-connected PV continues to present new challenges.

Reverse power flow

Distribution systems were originally designed and operated under the assumption that power flows from one point, the substation, out toward the customers. One implication of this is that voltage can be high near the substation and will drop further out from the substation unless it is boosted by a VR. The assumption of unidirectional power flow is up-ended by the addition of high levels of PV generation on the distribution system. When PV is added, power can flow from customer sites toward the substation. Reverse power flow can cause high voltages near the PV plant which may exceed ANSI limits if voltage controls are not adjusted to mitigate voltage rise.

PV Variability

PV output changes throughout the day based on the sun's location and cloud conditions. A PV plant's output can fluctuate quickly as clouds pass over the solar array. While customer loads change continuously throughout the day, the large number and diversity of loads tends to ensure that, in aggregate, the total load on a distribution system or even a given area of a distribution system changes slowly during normal operation. This means that voltage control devices can react fairly slowly as conditions change gradually; VRs and capacitors routinely have time delays between 30 seconds and 2 minutes. When a large PV plant is added, large changes in generation, and thus changes in net load can occur more rapidly. The impact of large rapid changes is two-fold. First, control devices with time delays on the order of minutes cannot keep pace with large changes that occur on the order of tens of seconds. Second, while large changes in load usually occur a few times a day (as people wake up, leave for work, come home, and go to bed), large changes in PV output can occur many times per hour as clouds pass. This means that devices which normally would incur a few operations per day need to operate many times each hour to adequately regulate voltages in the presence of highly variable PV generation [5]. This results in excessive wear and tear on those devices which may need to be maintained or replaced more often.

Potential for PV to improve grid operations

While PV can be seen as a detriment to distribution operations, PV plants equipped with smart inverters can mitigate the negative impacts while providing additional services. Smart inverters have volt-var control capabilities as required by the recent IEEE 1547 standard; they can adjust their power factor to supply or absorb reactive power as needed [6]. This ability

enables smart inverters to contribute to volt-var control. Furthermore, smart inverters can curtail real power which can mitigate voltage rise at critical times.

Increasing PV hosting capacity

The PV hosting capacity, or the amount of PV that can be added to a distribution feeder without impacting power quality, often is limited by voltage rise at low loading conditions [7]. However, with intelligent volt-var control, PV plants can mitigate their own voltage impacts and support additional grid services. This would provide benefits for both solar developers and utilities. From the utility perspective, the solar plants could contribute to volt-var control, which may reduce the need for investment in additional utility-owned control devices. In addition, with additional volt-var control provided by PV plants, the hosting capacity of a circuit could be increased. Increased hosting capacity opens up opportunities for developers to build more or larger PV plants on a given circuit. Additional PV generation on a well-planned circuit with adequate control would provide increased societal benefits in the form of low-emission generation.

Centralized Volt-var Control

Chapter 2 presents a centralized optimal volt-var control algorithm (CVVC) which coordinates customer-owned controllable loads and smart solar inverters with utility-owned voltage regulators and capacitors to meet voltage control objectives. The optimization problem is formulated as a mixed-integer nonlinear programming (MINLP) problem whose objective is to minimize the cost of all control actions as well as reduce voltage fluctuations. Constraints ensure that voltages remain within ANSI limits and power factor at the substation remains within the desired range. A voltage sensitivity matrix (VSM) is used to linearize the effect of control

actions on the voltage at customer nodes. The algorithm is tested using software simulations and using a real-time hardware-in-the-loop testbed.

Chapter 3 integrates the CVVC with a transmission controller to provide coordinated control on the distribution and transmission levels. The transmission controller, developed at Pacific Northwest National Lab (PNNL), relies on active and reactive power adjustments at the distribution level to provide voltage support to the transmission system. Chapter 3 details the changes to the CVVC required to integrate with the transmission controller. The integrated control framework is tested using a networked real-time simulation testbed.

Chapter 4 discusses necessary improvements to the CVVC algorithm discussed in chapter 2 so it can be feasibly implemented. First, the method in chapter 2 assumes full visibility of the voltage at every node of the system. The number of sensors and communication infrastructure required needs to be reduced for the system to be economically feasible. Next, implementation of optimal control actions using legacy utility-owned control devices must be addressed. Finally, significant computational power is needed to run hundreds of power flows to calculate the VSM and solve a large MINLP every 5 minutes. The computational power can be reduced by eliminating the need to calculate the VSM in real-time and reducing the MINLP constraints by focusing on critical nodes. With these improvements, the algorithm can be implemented on a grid-edge computing device with limited computational power.

Chapter 2: **VSM-Based DER Dispatch MINLP for Volt-Var Control in Unbalanced Power Distribution Systems**

This chapter presents a centralized volt-var control (CVVC) algorithm to coordinate customer-owned controllable loads and smart solar inverters with utility-owned voltage regulators and capacitors to meet voltage control objectives [8]. The optimization problem is formulated as a mixed-integer nonlinear programming (MINLP) problem. A voltage sensitivity matrix (VSM) is used to linearize the effect of control actions on the voltage at customer nodes when solving the MINLP. The VSM is recalculated at each time step to improve the computational accuracy. Both discrete switching actions of the capacitor and VRs and the continuous adjustment of real and reactive power from load and smart inverters are considered in the MINLP volt-var problem formulation. The objective function minimizes the cost of all control actions and the magnitude of voltage fluctuations from the previous time period. Constraints ensure that the voltage at each node is maintained within ANSI limits and the feeder power factor is controlled within the desired range. The algorithm is tested using an actual 3-phase unbalanced distribution feeder model. Simulation results demonstrate that the proposed algorithm is computationally feasible on real circuits and improves voltage control while minimizing operational costs.

Background and Literature Review

High penetration of solar generation on distribution circuits can cause violations of voltage standards, larger voltage fluctuations, and increased utility-owned device operations [5]. In high solar penetration circuits, voltage control is increasingly difficult if relying solely on traditional voltage control devices like capacitors, on-load tap changers (LTC) and line voltage regulators (VRs). Thus, it is increasingly important to develop advanced voltage control methods that coordinate all available resources to manage voltage in real-time.

While the integration of photovoltaics (PV) can worsen these voltage issues, PV inverters can provide reactive power for cheaper and more continuous voltage control than conventional resources. Combined with the smart controls for customer loads, these customer-owned distributed energy resources (DERs) can control voltages on feeders more precisely with smaller voltage fluctuations [9]. Conventional voltage control schemes utilize capacitors and VRs designed to meet control objectives during forecasted peaks only. As a result, capacitors and VRs have fixed local set points that are not adapted frequently in response to a wider range of system operation conditions (e.g., low and high loads, high and low PV production). In addition, control actions of VRs and capacitors are discrete (i.e., changing regulator taps and switching capacitors in/out), causing a large voltage fluctuation during each switching event. The mechanical switches and tap changers also accumulate wear-and-tear each time they operate.

Installing VR devices requires substantial capital investments, yet they are relatively inflexible and ill-suited to regulate fast changing voltages caused by high-penetration of variable solar generation resources. Therefore, there has been growing interest and research in developing DER-based volt-var control algorithms which utilize smart inverters and controllable loads in coordination with the utility-owned assets to regulate voltage variations [5], [9] - [10]. Several papers have used voltage sensitivity matrices (VSM) based on simulation results [9] or linearized power flow equations [11] - [12], [13] to effectively estimate the effect of control actions taken by utility- and consumer-owned resources. Coupled with optimization programs, VSMs have been shown to successfully control voltage using these assets [9], [14], [10]. Several of these have proven effective on circuits with high penetrations of PV [5], [9], [15], [16]. These methods have the advantage of being capable of controlling voltage in a more active manner in response to a wider range of operating conditions. However, the current research has been limited to small

IEEE test systems [17], [10], [16], systems with balanced phases [5], [10], [15], [16], and cases that use only a subset of the consumer- or utility-owned resources [9], [14], [16]. To fully utilize distribution resources, volt-var strategies need to schedule and operate multiple resource types concurrently and optimally. Thus, each resource needs to be weighted by its capability to regulate voltage variations and the cost of operation. Additionally, the method needs to be scalable so that optimal dispatch commands can be generated for distribution feeders consisting of hundreds of load nodes and smart inverter units in real-time.

Thus, a volt-var algorithm that optimizes the dispatch of customer resources including load and PV systems' real and reactive power along with VRs and capacitors is proposed in this chapter. The optimization problem is formulated as a mixed-integer nonlinear programming (MINLP) problem. A voltage sensitivity matrix (VSM) is used to linearize the effect of control actions on the voltage at customer nodes when solving the MINLP. The VSM is recalculated at each time step to reflect the latest operating condition, an improvement on the averaged VSM used in [9]. Both discrete switching actions of the capacitor and VRs and the continuous adjustment of real and reactive power from load and smart inverters are considered in the MINLP volt-var problem formulation. The objective function minimizes the cost of all control actions and the magnitude of voltage fluctuations from the previous time period. Constraints ensure that the voltage at each node is maintained within ANSI limits and the feeder power factor is controlled within the desired range.

The algorithm is tested on a 3-phase unbalanced distribution feeder model representing a real circuit in rural North Carolina. The feeder includes 998 buses, 371 of which are load buses. Simulation results demonstrate that the algorithm is effective, accurate, and computationally feasible for real-time applications.

MINLP-based CVVC Algorithm

We assume that a centralized DER and utility resource controller at the distribution control center will execute the volt-var control algorithm every 5 minutes. Customer-owned resources include controllable loads and PV systems with smart inverters. Utility-based resources include switched capacitors and LTC/VRs.

At the core of the volt-var control algorithm is the VSM-based linearized voltage calculation and the MINLP-based optimal dispatch. The MINLP determines the optimal schedule for each resource's operation for each time step by minimizing the cost of dispatch and the voltage change between time steps. The MINLP's constraints maintain voltage and power factor within the desired limits and customer- and utility-owned resources within their operating limits. The VSM approximates the voltage response across the circuit due to operation of the controllable resources so that we don't need to solve power flows for each MINLP iteration.

Voltage Sensitivity Matrix

The proposed VSM method accounts for current operating conditions by calculating a new set of sensitivity factors at the beginning of each 5-minute control interval. Note that we define L as the set of all controllable load nodes, K as the set of all PV nodes, $N = L \cup K$ as the set of all load and/or PV nodes, M as the set of all capacitor banks, and R as the set of all VRs, including the LTC at the feeder head. First, a power flow is run with current loads, PV outputs, capacitor status, and VR tap settings to calculate the voltages V_i^{Base} at each node i in N. Then, the real power injected at each node, j, in N is perturbed by a small value, ΔP, one node at a time, and the resulting voltages, $V_{i,j}^{P}$, for each node, i, in N are recorded. The sensitivity factors with respect to real power injection are calculated using (1). Similarly, the voltage sensitivity to reactive power is calculated by perturbing the reactive power injected at each node, j, in N by a

small value, ΔQ, and recording the resulting voltages, $V_{i,j}^{Q}$, for use in equation (2). To find the sensitivity to capacitor switching, the status of each capacitor, m, in M is toggled from its current position, one at a time, and the resulting voltages, $V_{i,m}^{cap}$, for each node, i, in N are recorded and used in equation (3). Finally, the sensitivity to tap changes is calculated by adjusting the position of each VR, r, in R up one tap and recording the resulting voltages, $V_{i,r}^{VR+}$, for use in equation (4). The VRs are also adjusted down one tap to calculate the voltage sensitivity in that direction using equation (5). All voltages are calculated using full power flow solutions.

$$VSM_{i,j}^{P} = \frac{V_{i,j}^{P} - V_i^{Base}}{\Delta P} \qquad \forall i \in N, \forall j \in N \tag{1}$$

$$VSM_{i,j}^{Q} = \frac{V_{i,j}^{Q} - V_i^{Base}}{\Delta Q} \qquad \forall i \in N, \forall j \in N \tag{2}$$

$$VSM_{i,m}^{Cap} = V_{i,m}^{cap} - V_i^{Base} \quad \forall i \in N, \forall m \in M \tag{3}$$

$$VSM_{i,r}^{VR+} = V_{i,r}^{VR+} - V_i^{Base} \quad \forall i \in N, \forall r \in R \tag{4}$$

$$VSM_{i,r}^{VR-} = V_{i,r}^{VR-} - V_i^{Base} \quad \forall i \in N, \forall r \in R \tag{5}$$

Mixed-Integer Nonlinear Program

At each time step, a convex MINLP is solved to determine optimal dispatch for each controllable resource. The problem is solved using the BONMIN solver. The objective of the MINLP is to minimize the cost of load control, PV curtailment, capacitor switching, and VR tap changes while reducing changes in voltage from one period to the next. The objective function contains a term for the cost of voltage deviation from the previous period which reflects benefits from limiting swings in voltages between time periods.

$$\min \sum_{i\in L} C_i^L + \sum_{k\in K} C_k^{PV} + \sum_{m\in M} C_m^{cap} + \sum_{r\in R} C_r^{VR} + \sum_{i\in N} \alpha_{\Delta V} \times [V_i^{t-1} - V_i(\cdot)]^2 \quad (6)$$

Subject to:

$$0 \le \Delta P_i^{L+} \le \overline{P_i^{L+}} \qquad \forall i \in L \quad (7)$$

$$0 \le \Delta P_i^{L-} \le \overline{P_i^{L-}} \qquad \forall i \in L \quad (8)$$

$$0 \le \Delta P_k^{PV} \le \overline{P_k^{PV}} \qquad \forall k \in K \quad (9)$$

$$\frac{\left(\mathrm{Q^{Base}} + \sum_{k\in K} \Delta \mathrm{Q_k^{PV}} + \sum_{i\in L} (\Delta P_i^{L+} - \Delta P_i^{L-}) \times \frac{\sqrt{1-pf_i^{L\,2}}}{pf_i^L} - \Delta Q^{Cap}\right)^2}{\left(\mathrm{P^{Base}} + \sum_{k\in K} \Delta \mathrm{P_k^{PV}} + \sum_{i\in L} (\Delta P_i^{L+} - \Delta P_i^{L-})\right)^2} \le \frac{1-pf^2}{pf^2} \quad (10)$$

$$(\Delta Q_k^{PV})^2 \le 1.1 \sqrt{(S_k^{PV})^2 - \left(\overline{P_k^{PV}} - \Delta P_k^{PV}\right)^2} \quad \forall k \in K \quad (11)$$

$$\underline{V} \le V_i(\cdot) \le \bar{V} \qquad \forall i \in N \quad (12)$$

$$\Delta T_r^- + \Delta T_r^+ \le 1 \qquad \forall r \in R \quad (13)$$

$$\Delta T_r^-, \Delta T_r^+, \Delta S_m \in \{0,1\} \quad \forall r \in R, m \in M \quad (14)$$

Note that

$$V_i(\cdot) = V_i^{Base} + \sum_{j\in N} VSM_{i,j}^P \times \left(\Delta P_j^{L+} - \Delta P_j^{L-} - \Delta P_j^{PV}\right)$$

$$+ \sum_{j\in N} VSM_{i,j}^Q \times \left(\Delta Q_j^{PV} + \frac{\sqrt{1-pf_j^{L\,2}}}{pf_j^L} \times \left(\Delta P_j^{L+} - \Delta P_j^{L-}\right)\right)$$

$$+ \sum_{m\in M} VSM_{i,m}^{Cap} \times \Delta S_m + \sum_{r\in R} (\Delta T_r^+ \times VSM_r^{VR+} + \Delta T_r^- \times VSM_r^{VR-}) \quad (15)$$

and

$$\Delta Q^{Cap} = \sum_{m\in M'} \Delta \mathrm{S_m} \times Q_m^{Cap} - \sum_{m\in M''} \Delta \mathrm{S_m} \times Q_m^{Cap} \quad (16)$$

where $\overline{P_i^{L+}}$ and $\overline{P_i^{L-}}$ are the maximum controllable load increase and decrease at node i, respectively; $\overline{P_k^{PV}}$ is the maximum curtailable PV at node k; Q^{Base} and P^{Base} are the reactive and real power delivered to the circuit in the initial power flow before control; pf_i^L is the power

factor of load at node i; pf is the desired power factor limit at the feeder head; S_k^{PV} is the rated capacity of PV at node k; $\underline{V}$ and $\bar{V}$ are the desired minimum and maximum voltage limits at all load nodes; $V_i(\cdot)$ is the estimated voltage at a node i after controls; and V_i^{t-1} is the voltage at node i from the previous time step's power flow solution. M' is the set of capacitors that are off and M'' is the set of capacitors that are on. Q_m^{Cap} is the kvar rating of capacitor m. The decision variables are $\mathbf{\Delta P^{L+}}$ and $\mathbf{\Delta P^{L-}}$, the vector of increase or decrease in load at all load nodes; $\mathbf{\Delta Q^{PV}}$, the vector of reactive power absorbed at all PV nodes; $\mathbf{\Delta P^{PV}}$, the vector of real power curtailment at all PV nodes; $\mathbf{\Delta S}$, the vector of the changes in all capacitor statuses; and $\mathbf{\Delta T}^-$ and $\Delta\mathbf{T}^+$, the vectors of negative or positive tap change at all VRs.

Equations (7-8) limit the real power increase and decrease at each controllable load to 20% of the unadjusted load at that node. Equation (9) limits the real power curtailment at each PV node to the current PV output at that node. Equation (10) constrains the power factor at the top of the feeder to limit excessive reactive power pushed to the transmission system. Equation (11) constrains the total real and reactive power from each PV system within its capacity. For this study, each inverter is sized such that its total apparent power can be up to 110% of its rated real power capacity, which increases the amount of reactive power that can be provided. Equation (12) limits voltage at all nodes to distribution ANSI limits. Equation (13) ensures that each VR cannot adjust up and down simultaneously in the model. Equation (14) restricts the tap change and capacitor switch variables to discrete values. Equation (15) uses the VSM to approximate the resulting voltage after control actions. Equation (16) gives ΔQ^{Cap}, the total change in reactive power injected by capacitors.

Resource Cost Functions

The cost functions of resources determine how the resources are dispatched in the MINLP. The formulations of the control cost functions are chosen to represent their price to the distribution operator and customer preferences.

Load Cost: In our feeder model, load nodes represent aggregated demand of multiple (5-10) customers. The diversity of loads allows for an assumption of continuous quantities of demand response (DR). In addition to modeling load reduction as a resource, this study assumes that the utility can motivate customers to increase load when needed. The model does not include any rebound effect representing load which is curtailed (or increased) in the current period being shifted to increased demand (or reduced demand) in the future. The cost curves of DR are represented as

$$C_i^L = \frac{\alpha_{Load}}{P_i^L} \times (\Delta P_i^{L+} + \Delta P_i^{L-})^2 \qquad \forall i \in L \tag{17}$$

Where P_i^L is the unadjusted load at node I and α_{Load} is a weighting factor for the cost of load deviations.

The quadratic cost function reflects increasing marginal costs with respect to quantity of DR acquired. The quadratic coefficient is dependent on the unadjusted load at the current time step to represent a higher marginal cost for loads with fewer customers (lower aggregated load) and at low load periods.

PV Cost: PV plant owners are assumed to accept prices for real power curtailment which are equal to the price for which they would have sold the power.

$$C_k^{PV} = \alpha_{PV} \times \Delta P_k^{PV} \qquad \forall k \in K \tag{18}$$

Inverter-supplied reactive power is not costed directly. However, there is an opportunity cost for reactive power injection or absorption when it requires PV curtailment. Equation (11) models this relationship.

VR and Capacitor Cost: Unlike PV and load operation costs, capacitor and VR operational costs are influenced by the number of switching or tap changing events. Frequent operation of these devices can lead to increased maintenance and replacement costs. So, those devices have a constant price per operation given by

$$C_m^{cap} = \alpha_{cap} \times \Delta S_m \qquad \forall m \in M \tag{19}$$

$$C_r^{VR} = \alpha_{VR} \times \Delta T_r \qquad \forall r \in R \tag{20}$$

where α_{cap} and α_{LTC} are the costs of one capacitor switch or tap change, respectively.

The optimization parameters are listed in Table 2.1. Note that the voltage limits are set slightly inside the ANSI limits to allow for a small amount of error in linearized voltage estimates.

Table 2.1. Optimization Parameters Used in Case Study

Parameter	Value	Parameter	Value
$\boldsymbol{\alpha_{PV}}$	0.005	Q_p	5 kvar
$\boldsymbol{\alpha_{QPV}}$	0.0001	P_p	5 kW
$\boldsymbol{\alpha_{VR}}$	0.5	$\bar{V}$	1.04 pu
$\boldsymbol{\alpha_{Load}}$	0.1	$\underline{V}$	.975 pu
$\boldsymbol{\alpha_{\Delta V}}$	0.5	$\overline{P^{L+}}$	20% of base
$\boldsymbol{\alpha_{cap}}$	0.1	$\overline{P^{L-}}$	20% of base
pf	0.98	$\overline{P_k^{PV}}$	100% of current output

Software Simulation Setup

A real 3-phase unbalanced distribution feeder (see Figure 2-1) in rural North Carolina is modeled in OpenDSS to perform the case study [18]. This feeder topology reflects typical

distribution circuit expansions after progressive upgrades over years of load growth. Unlike IEEE test systems, the circuit has multiple long single-phase taps, making balancing load among phases difficult. Note that those phase imbalances often lead to single-phase control actions to keep voltages on all phases within limits. As shown in Figure 2-1, the utility-owned assets include an LTC at the feeder head, one three-phase regulator, two single-phase regulators, and a three-phase 600 kvar capacitor bank. The LTC and voltage regulators are set to regulate at 125V with a dead band of ±1 V and a time delay between 30 and 90 seconds.

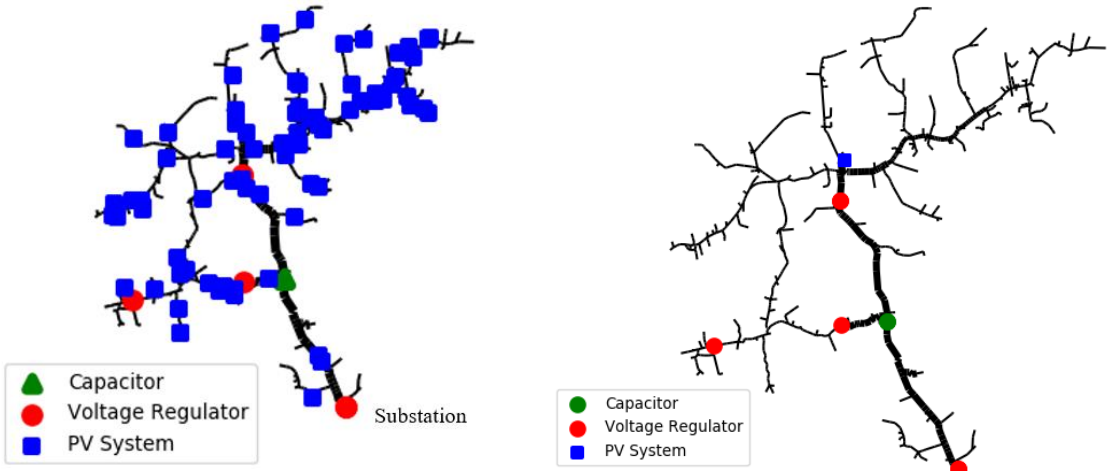

(a) (b)

Figure 2-1. Topology of a rural distribution feeder in North Carolina with 100% residential PV penetration (a) and 100% utility-scale PV penetration (b)

We use the hourly feeder-head load profile collected at the substation during one winter week in 2016 with the feeder load disaggregation algorithm presented in [19] to allocate 5-minute resolution load profiles to each load node. This step is crucial to give each load node a realistic individual load profile while ensuring that the aggregated load matches the measured feeder-head load profile.

PV was added to create two cases with 100% PV penetration: a residential PV case and a case with a single utility-scale PV plant. To create the residential (distributed) PV penetration

case, we add residential PV systems randomly to load nodes throughout the feeder until the total PV capacity reaches 100% of the peak load. The PV system generation profiles are chosen from 147 residential PV profiles recorded by the Pecan Street project [20]. The power rating of each PV systems ranges from 3 kW to 10 kW. We assume that each PV system is equipped with a smart inverter that can inject and absorb reactive power. The resulting substation load, PV, and net load profiles are shown in Figure 2-2.

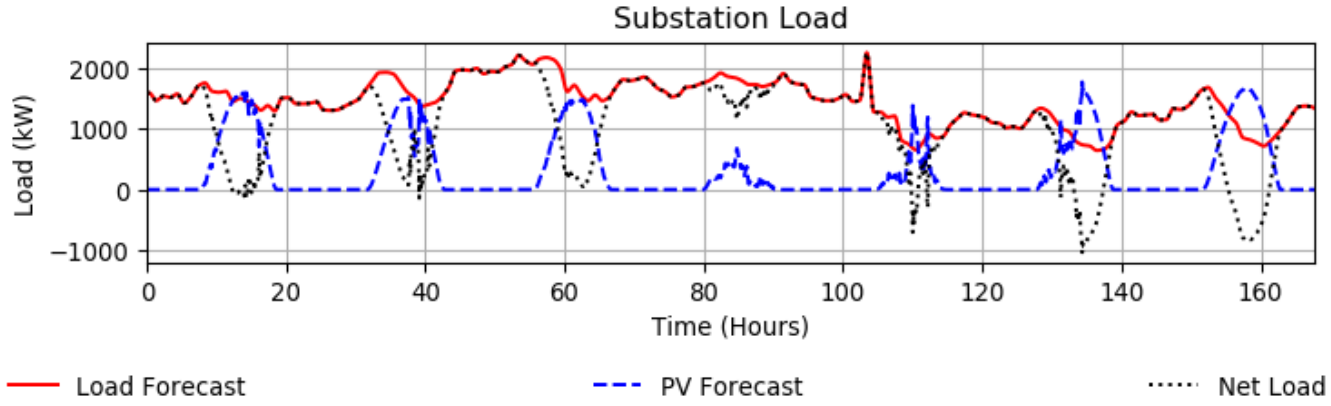

(a)

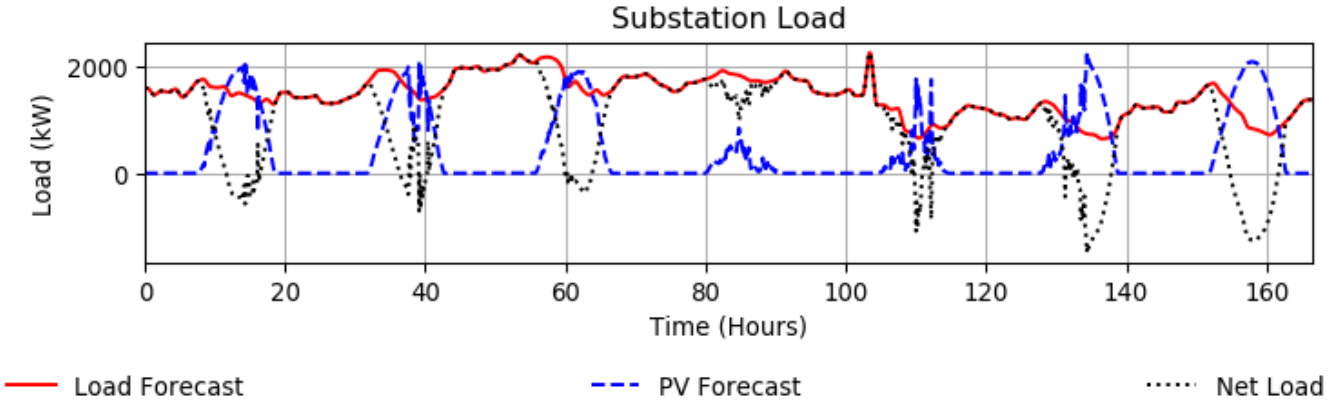

(b)

Figure 2-2. PV and net load for one winter week with 100% residential (a) and utility-scale (b) PV

To create the utility-scale PV case, we add a single 3-phase PV plant near the end of the circuit with capacity equal to the peak load. A single Pecan Street PV profile is scaled up to match the PV system capacity.

In the base case, only utility-owned assets (i.e. LTC, VRs, and capacitor banks) are used to control voltage. The simulation runs for one week with 10-second time steps to capture the control actions of the voltage regulation devices with time delays under 5 minutes. Then, the results are down-sampled to 5-minute intervals to compare with the optimally controlled case.

In the optimally controlled case, the proposed CVVC algorithm is used to regulate voltage for the same week at a 5-minute control interval. In this case, loads, PV real and reactive power, regulators and capacitors were optimally dispatched based on the VSM-based MINLP algorithm.

Software Simulation Results

Accuracy of the VSM-based Voltage Calculation

The accuracy of the voltage calculation using the VSM is crucial to the effectiveness of the voltage regulation as well as the computational speed of the algorithm. Figure 2-3 and Figure 2-4 show the difference between the estimated node voltages calculated during the optimization and the actual voltages calculated through power flow simulation after performing control operations prescribed by the optimization. The error is below 10^{-2} per unit, which is within the error threshold for distribution operations.

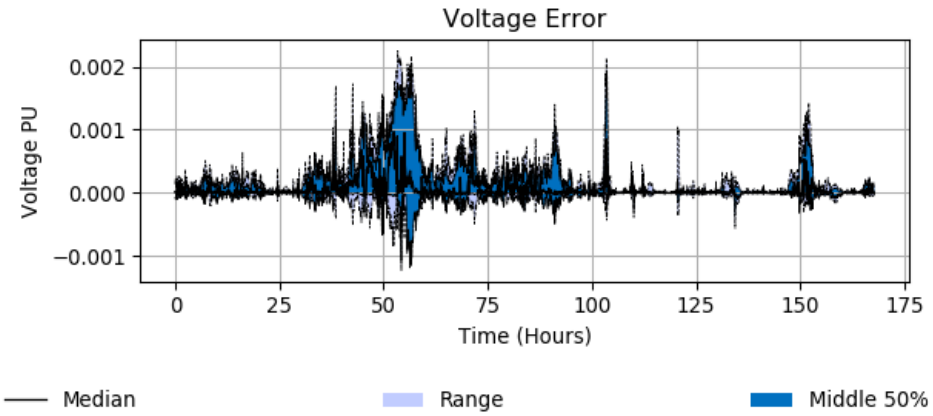

Figure 2-3. Error between nodal voltages calculated using VSM and power flow for the Residential PV case

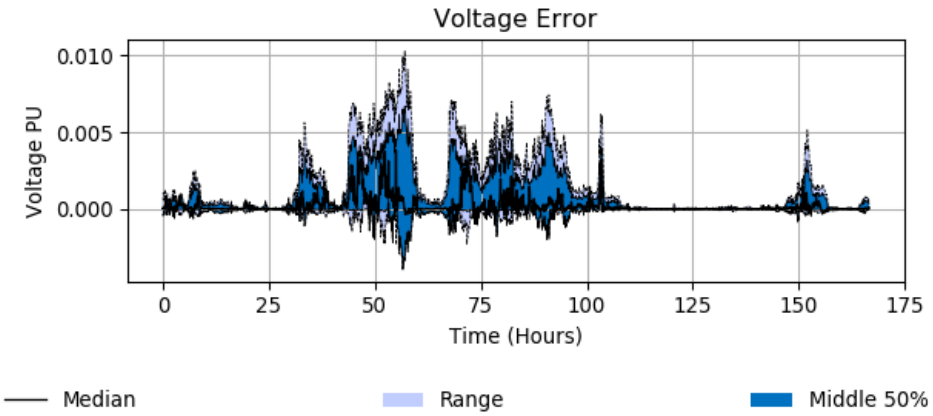

Figure 2-4. Error between nodal voltages calculated using VSM and power flow for the utility-scale PV case

Voltage Regulation

Figure 2-5 and Figure 2-6 show the distribution of the nodal voltage at each time step for the base case and with the VSM control method for the residential and utility-scale cases, respectively. In the base case, the existing control scheme is not able to maintain all nodal voltages within the desired range. In the optimal control case, there are very few voltage violations. The optimal control case also shows less frequent and less rapid voltage fluctuations due to the voltage fluctuation penalty in the objective function.

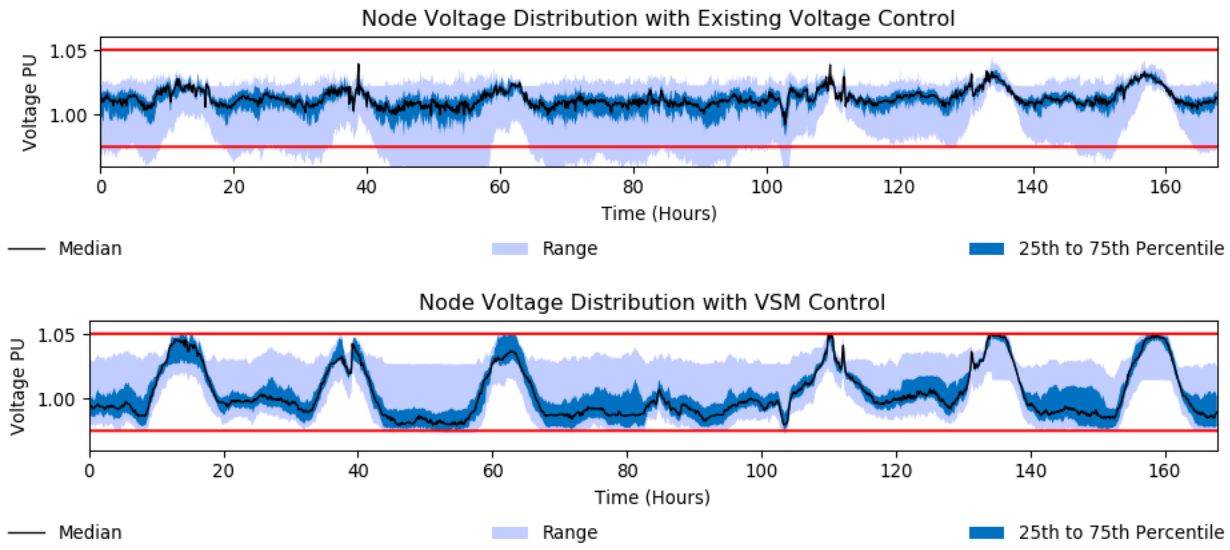

Figure 2-5. Range, middle 50% and median node voltages at each time step

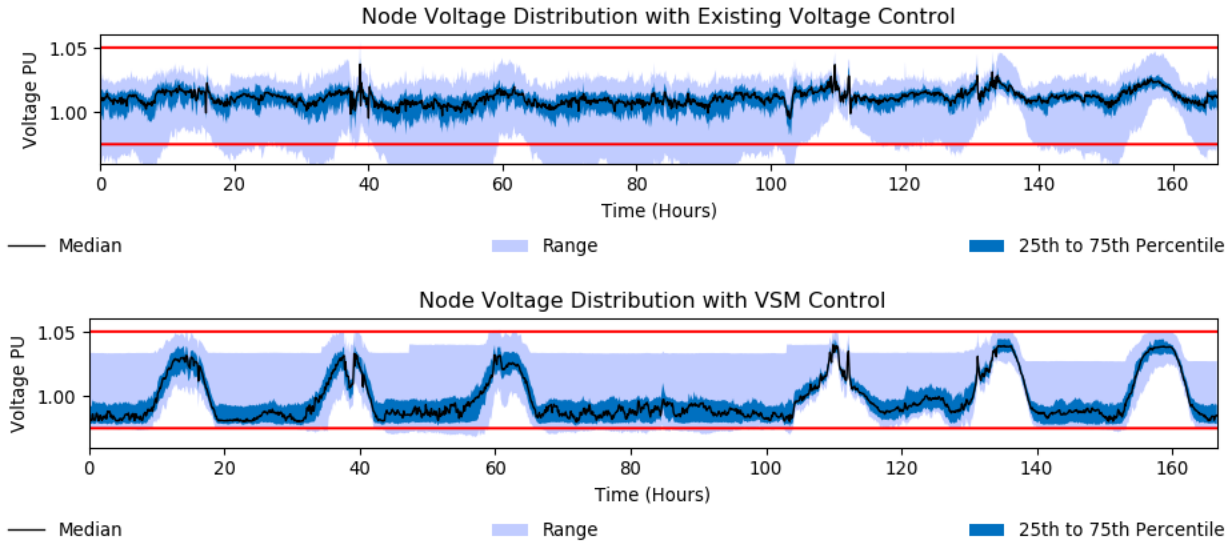

Figure 2-6. Range, middle 50% and median node voltages at each time step

Figure 2-7 shows how smart inverter reactive power output and demand response are used to correct voltages throughout the week for each case. In the utility-scale PV case, higher magnitudes of reactive power are needed because the single PV plant can only provide reactive power in one location. In the residential PV case, reactive power can be injected from the most impactful residential PV systems (usually those closest to the voltage issue). Therefore, the

amount of reactive power needed to correct a voltage issue is often lower in the residential PV case.

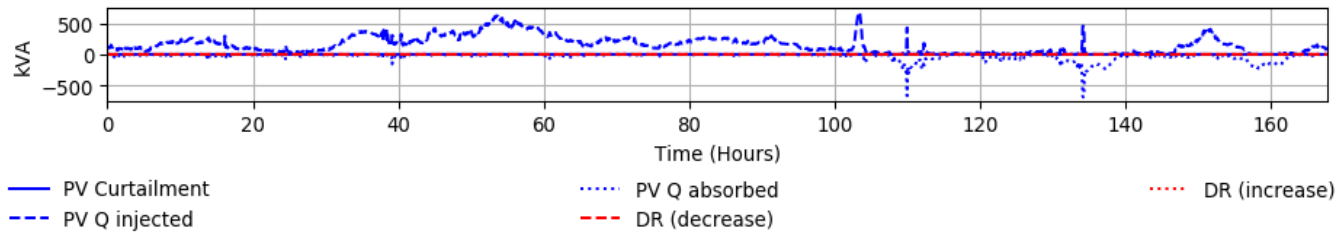

(a)

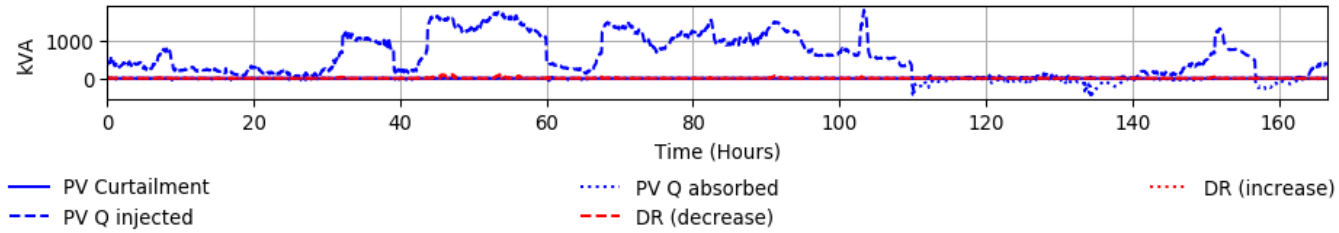

(b)

Figure 2-7. Optimal control actions for one week with residential (a) and utility-scale (b) PV

Since this method uses significant reactive power injection and absorption to regulate voltages, power factor can become a concern. In Figure 2-8, we can see that by including a constraint on power factor at the top of the feeder within the MINLP, the power factor is successfully maintained between .98 leading and .98 lagging throughout the simulated week despite heavy use of reactive power.

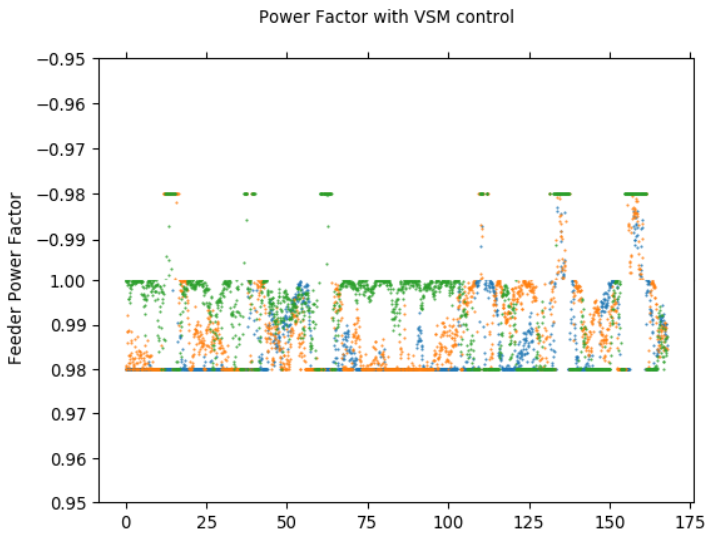

(a)

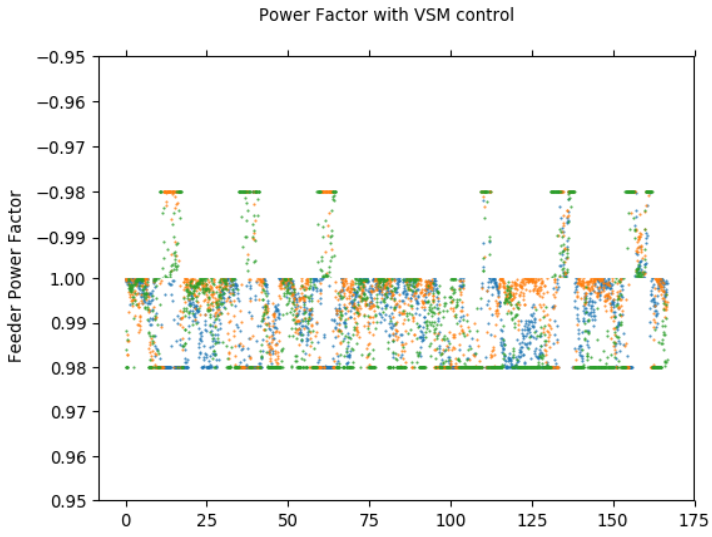

(b)

Figure 2-8. Power factor at the substation with optimal control for the residential (a) and utility-scale (b) PV cases

Table 2.2 compares the total amount and cost of all control actions for each case. In both cases, the cost of the control is vastly reduced when using the optimization rather than the traditional control which only employs locally-controlled VRs and capacitors. Most of the control is accomplished using very cheap reactive power from the smart inverters rather than costly tap changes and capacitor switches. Note that much of that control is accomplished with

little PV curtailment. This is possible when inverters are slightly oversized compared to the PV array so that there is always some capacity available for reactive power.

Table 2.2. Overall number or quantity of each control action and their costs for the base case and optimal case.

Residential PV Case				
	Existing Control		VSM Control	
	Actions	Costs	Actions	Costs
Capacitor Switches	0	$ 0.00	0	$ 0.00
Tap Changes	571	$ 285.50	2	$ 1.00
PV Curtailment (kWh)	-	-	9.87	$ 0.59
Inverter Q Injection (kvarh)	-	-	24,846.91	$ 2.98
Inverter Q Absorption (kvarh)	-	-	5,100.86	$ 0.61
Demand Response (kWh)	-	-	17.56	$ 0.01
Total Cost		$ 285.5		$ 5.20
Utility-scale PV Case				
	Existing Control		VSM Control	
	Actions	Costs	Actions	Costs
Capacitor Switches	0	$ 0.00	8	$ 0.80
Tap Changes	684	$342.00	5	$ 2.50
PV Curtailment (kWh)	-	-	10.15	$ 0.61
Inverter Q Injection (kvarh)	-	-	91,681.43	$ 11.00
Inverter Q Absorption (kvarh)	-	-	4,130.94	$ 0.50
Demand Response (kWh)	-	-	602.08	$ 18.51
Total Cost		$342.00		$ 33.92

Computational speed

Finally, we consider the computational time necessary to calculate the VSM and optimize resource dispatch. This metric determines whether it is possible to run this algorithm in real time as an operational tool. Figure 2-10 shows a boxplot of the computational time to calculate the VSM and solve the MINLP for each time step. All time steps are completed well within the 5-

minute requirement and the majority of scenarios run in under one minute on a computer with an intel i7-4770 processor. The residential PV case generally takes longer because there are more variables associated with the large number of PV systems compared with a single PV system in the utility-scale case.

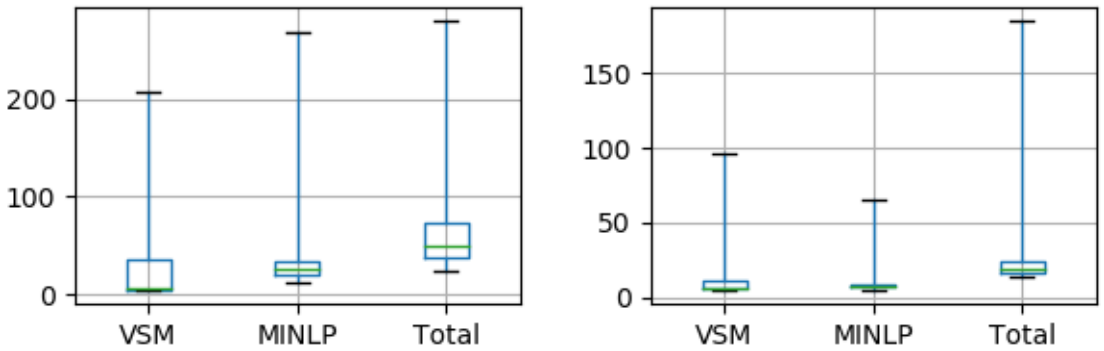

(a) (b)

Figure 2-9. Boxplots showing the median (line), 25th and 75th percentiles (box) and range (whiskers) for time to calculate the VSM, time to solve the MINLP, and the total run time for each time step for the residential (a) and utility-scale (b) PV cases.

Real-Time Simulation Setup

In the previous section, the performance of the CVVC algorithm is validated via a steady-state-power-flow-based simulation tool with an assumption of no communication delays between the CVVC controller and DERs. In this section, a hardware-in-the-loop (HIL) platform is used to simulate the CVVC [21]. This testbed allows DER control methods to be developed and tested on a platform that simulates transients inside each subsystem (e.g., an energy storage device or a PV farm) and dynamics of the entire grids (i.e., from distribution feeders to transmission systems). Communication links between the centralized controller and the DER controllers are established using actual communication protocols and simulators to enable the modeling of realistic communication and control delays.

The Configuration of the HIL Testbed

The configuration of the asynchronous HIL co-simulation platform is shown in Figure 2-10.

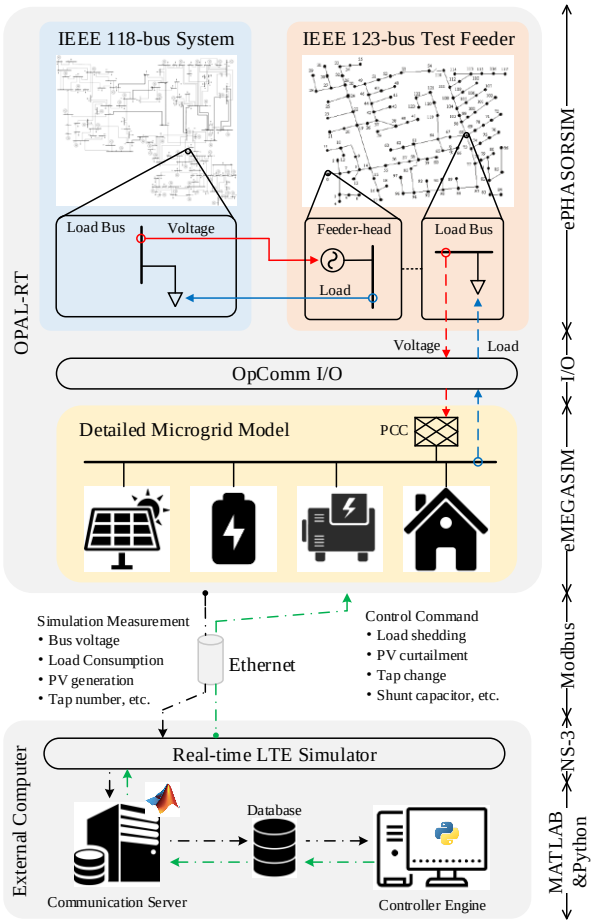

Figure 2-10. Architecture of the asynchronous HIL co-simulation platform.

The power distribution grid is modeled by the IEEE 123-node test feeder using ePHASORSIM with the simulation step size at the millisecond-level. The software can conduct power flow calculations for both unbalanced and balanced, 3-phase and 1-phase circuits in a distribution system. Because dynamic models of generators, capacitor banks, and motor loads are included, the ePHASORSIM-based test system can model the system transient response at the millisecond-level. Distributed energy resources, such as PV systems with smart inverters, are modeled using eMEGASIM so that their dynamic responses can be modeled with the

microsecond-level. In this paper, the simulation time step for eMEGASIM is set as 100μs and for ePHASORSIM as 10ms to balance the computational needs between speed and accuracy [21].

As shown in Figure 2-10 two communication connections are set up to model the communication between the device level controller and the centralized controller. The Ethernet protocol that can model several communication links connect the OPAL-RT simulator and an external computer. An LTE simulator is used to model wireless communication network. Communication links between OPAL-RT and LTE simulator is built using a Modbus connection. More details on the testbed setup can be found in [21].

Two types of controllable load model are used: 1-phase load and 3-phase unbalanced load. Each load is assigned a unique second-by-second profile designed from actual residential and commercial load profiles. The real power of the 1-phase load is received from the assigned load profile and the reactive power is calculated using the assigned power factor.

On this testbed, 95 distribution loads are modeled. Four out of the 95 loads are modeled by detailed 3-phase composited ZIP models, and the rest are modeled by assigned load profiles.

Three three-phase, 1.8MVA PV systems are modeled on the testbed. PV arrays are modeled by the equivalent circuit model in [22]. Converters are equipped with maximum power point tracking controllers. A 3-phase inverter is connected between the grid and the converter. A standard DQ controller is used for each phase so that the active and reactive power of each phase can be controlled separately by the CVVC controller.

The CVVC controller is modeled externally to the HIL based testbed. Although the controller makes decisions every 5 minutes, the HIL-based testbed is modeled in much finer detail. This allows the dynamic response of each subsystem caused by the control actions and their interactions to be simulated.

Ethernet and wireless connections are used to simulate the communication links between the CVVC controller (modeled on the external computer) and the local controllers (modeled on the HIL testbed) for controlling the smart inverters and VR devices. A Modbus point list is built based on the observable and controllable variables at each local controller module. Thus, the CVVC controller can only access those listed local controllable and observable variables. The controller inputs include voltage measurements at each load and PV node and at the substation; real and reactive power consumption by each load and injection by each PV system; capacitor statuses; switching states of on-load tap changers (LTCs) and tap positions of line voltage regulators.

One of the most important advantages to conducting real-time simulation is the capture of realistic communication and control delays on control efficacy, which is difficult to capture using quasi-static simulations.

As shown in Figure 2-11, at the beginning of each control interval, data produced by the real-time simulation test system on OPAL-RT are sent through communication links to the external controller. After the controller calculates the optimal control actions, the corresponding commands are sent back to the controllable devices modeled on the HIL testbed through the same links. The total time delay from when the measurements are taken to when the control actions are implemented can be up to 60 seconds, including the round-trip data propagation delay on Modbus and LTE network, which is less than 5 seconds, and the data recovery and control computation time, which varies from 15 to 60 seconds. If the control interval is every 5 minutes, each command will be in effect for approximately 5 minutes (from the time a control action is received at t = 60 s to the time it is updated at t = 360 s). Because the models on OPAL-RT are simulated at a small time step, the real-time simulation has already advanced many steps during

the 360 seconds and the load and PV injections may have changed. Thus, a control action calculated using data collected at $t = 0$ s may no longer be an optimal or even acceptable action to resolve all the voltage issues during that control interval, as is often observed in real-world implementation.

To mitigate the degradation on control efficacy caused by communication and control delays, the voltage dead band allowed in the optimization within the CVVC at the distribution control center is tightened by adjusting the minimum and maximum voltage constraint defined by (12). Once the voltages are initially corrected to within the tighter voltage deadband, the nodal voltage can vary as loads and PV outputs change but will remain within the ANSI limits throughout the control interval. However, narrowing the voltage deadband comes at a higher cost because more voltage control resources need to be called into action to satisfy the stricter constraints.

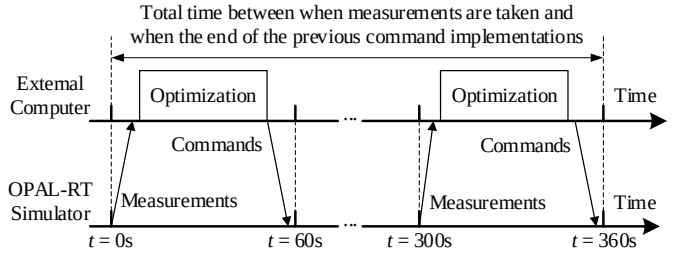

Figure 2-11. Control timeline for two control intervals.

To balance the likelihood of violating voltage constraints and the control cost, the voltage margin can be selected based on the expected voltage changes on a circuit. For example, the voltage margin is selected as 0.014 p.u., which is the 99th percentile of voltage change magnitudes occurring on all nodes across all 6-minute rolling intervals for one-day run without control.

By tightening the voltage constraints in the controller's MINLP by this margin, the controller can maintain all nodal voltage within the hard limits in the entire control period.

Real-time Simulation Results

The first test test demonstrates the HIL real-time simulation with and without the proposed VSM-based CVVC to demonstrate the effectiveness of the control strategy. The one-minute distribution of the nodal voltage without control and with the CVVC from 12:00 to 22:00 is summarized in Figure 2-12. Both cases have a perfect communication link without any interruption and the CVVC case has a control voltage margin (0.014 p.u.). The total number of voltage violations (TNVV) and the max voltage violation magnitude (MVVM) are used as the evaluation metrics. In the no control case, nodal voltage violates the allowed range [0.975, 1.05], with the TNVV as high as 21043 and the MVVM as 0.0326 p.u. In the control case, node voltages are limited within the required range and both TNVV and MVVM are zero.

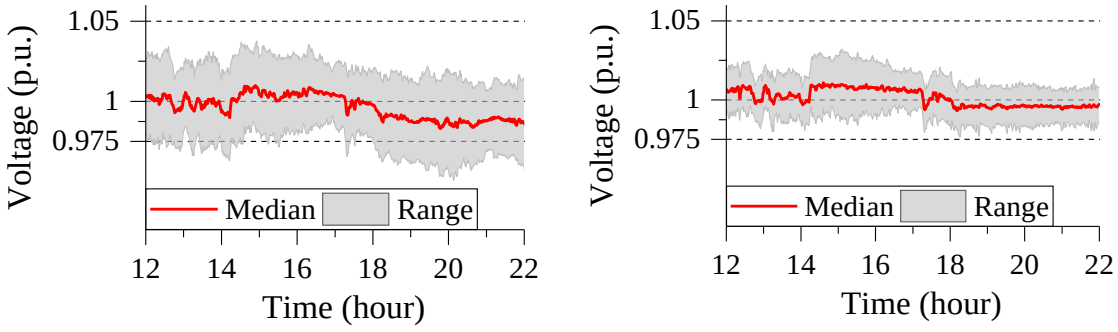

Figure 2-12. Nodal voltage profiles: (a) no-control baseline case and (b) controlled case with perfect communication.

Next, the impact of different voltage margins is demonstrated. Three 10-hour test cases are conducted assuming perfect communication. As shown in Table 2.3, when the voltage margin increases, there are more control actions taken to bring the voltages inside the tighter limit. As shown in Figure 2-13, if no voltage margin is used, nodal voltage will drop below the desired voltage lower limit. While setting up a large voltage margins (e.g., 0.02 p.u.) can remove nearly all voltage violations, it leads to frequent control actions, causing higher wear-and-tear a

higher control cost. Therefore, in practice, a suitable voltage margin (in this case, 0.014 p.u.) needs to be selected so that voltage violations can be removed with minimum increase in the number of control actions.

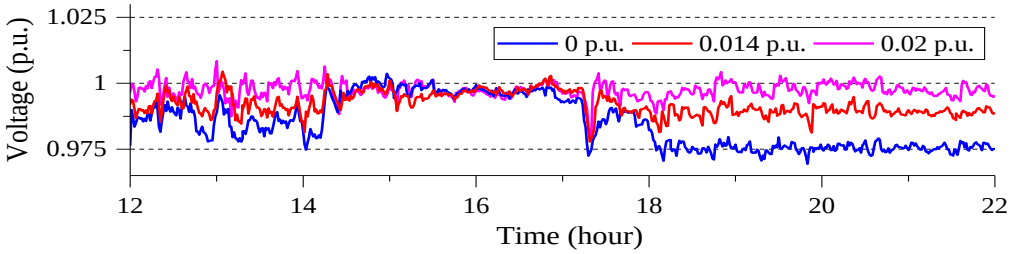

Figure 2-13. Phase *a* voltage at Node 50 when using different voltage control margins

Table 2.3. Summary of Simulation Results for Different Margins

Metrics	**Quantity**		
Voltage Margin (p.u.)	0	0.014 (99th percentile)	0.02
Voltage Limits (p.u.)	[0.975, 1.05]	[0.989, 1.036]	[0.995, 1.03]
DR down (kWh)	4.1	5.2	29.8
DR up (kWh)	0	0	0
Tap Changes (#)	0	0	1.0
Cap Switches (#)	0	0	0
PV curtailed (kWh)	0	0	0
PV Q injected (Mvarh)	7.8	14.5	24.4
PV Q Absorbed (Mvarh)	0	0	7.8
Cost ($)	1.07	1.13	5.10
TNVV	1702	0	2
MVVM (p.u.)	0.0116	0	0.0005

Discussion

The software and real-time simulation results demonstrate that the proposed method can improve voltage control while minimizing operational costs. This method can be adapted for various distribution system operators based on their specific costs and operational goals. For example, this method could be used to deploy conservation voltage reduction by lowering the desired maximum voltage constraint in the MINLP. Likewise, utilities with different operational

costs for PV curtailment, load participation, and utility-owned device operations can adjust the cost parameters to match their situation. Therefore, this method is highly versatile and could be employed by any DSO that has some or all of the devices mentioned.

The main limitation of this method is the need for extensive communication infrastructure for full visibility of the distribution system in real-time. Additionally, the recalculation of the voltage sensitivity matrix and solving the entire MINLP every 5 minutes is computationally intensive, especially considering the limited computational power of low-cost grid-edge computing devices. Chapter 4 will address these challenges and propose methods for reducing the required measurement, communication and computational resources.

Chapter 3: **Chapter 3: Coordinated Real-Time Sub-Transmission Volt-Var Control Tool (CREST-VCT)**

As DER penetration increases on distribution systems, the aggregated effects of DERs can begin to impact the transmission system. Reverse power flow from distribution feeders can cause unexpected voltage issues on the transmission system. However, coordinated volt-var control between the transmission and distribution can mitigate DER impacts at both levels. In this chapter, the CVVC algorithm in chapter 2 is extended to coordinate with a transmission volt-var controller. The resulting Coordinated Real-time Sub-Transmission Volt-var Control Tool (CREST-VCT) is illustrated in Figure 3-1. The operational timeline is shown in Figure 3-2. The focus of this chapter is the operation of the distribution-side controller within the integrated framework.

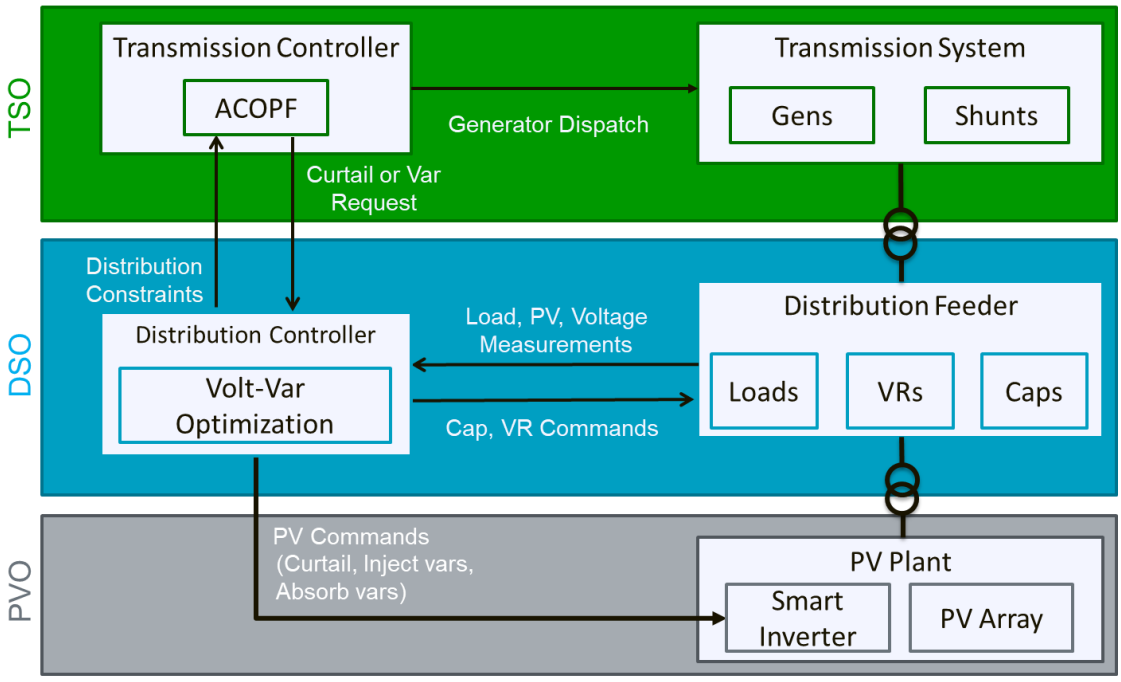

Figure 3-1. CREST-VCT Operational Framework

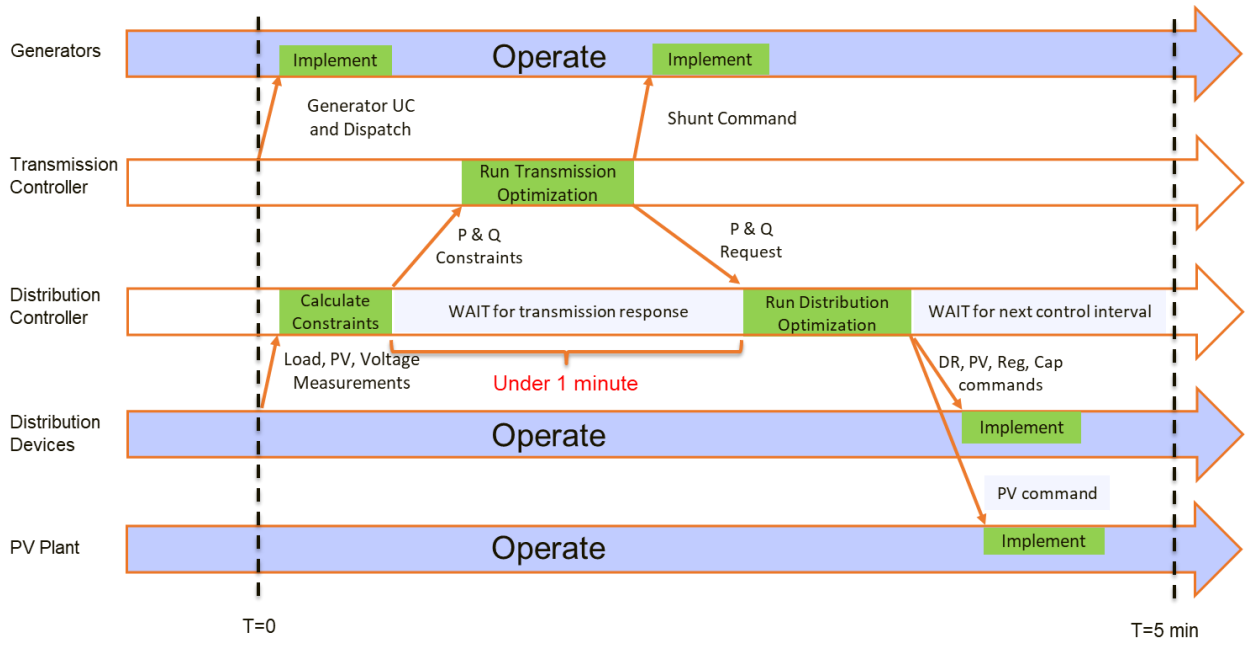

Figure 3-2. CREST-VCT Operational Timeline

The transmission volt-var controller consists of an ACOPF where the decision variables include generator set-points and shunt switches as well as changes in active and reactive power absorbed by each distribution substation. The transmission controller ACOPF constraints include the maximum adjustment up and down for active and reactive power at each substation.

On the distribution side, a distribution controller equipped with the CVVC algorithm is installed at each substation. At the beginning of each control iteration, the distribution controller gathers measurements from each controllable device within the substation's service area. Using those measurements and the device constraints, the total amount of active and reactive power adjustment available is calculated as the sum of each individual device's adjustment capacity. The distribution controllers send the constraints to the transmission controller, which solves the ACOPF. Then, the transmission controller sends the optimal set points to the transmission-level devices and the distribution active and reactive adjustment requirements to each substation's distribution controller. Finally, the distribution controller solves the coordinated CVVC and

sends the optimal commands to each device, which will correct any voltage issues and provide the requested power adjustment at the substation.

Distribution Optimization Formulation

The distribution-side CVVC optimization is nearly identical to that discussed in chapter 2. To incorporate transmission requirements, the power factor constraint (10) is replaced with (21) and (22) which forces the changes in active power and reactive power due to all control actions to be equal to the transmission requests ΔP^T and ΔQ^T.

$$\Delta P^T = \sum_{i \in L} \Delta P_i^{L+} - \Delta P_i^{L-} - \sum_{k \in K} \Delta P_k^{PV} \quad (21)$$

$$\Delta Q^T = \sum_{k \in K} \Delta Q_k^{PV} - \Delta Q^{Cap} \quad (22)$$

With this change, the CVVC can supply the optimal demand response needed for transmission operation while maintaining distribution-side voltages within the desired limits.

Real-time Test Setup

Building on the real-time testbed discussed in chapter 2, a networked HIL testbed was developed to test the CReST-VCT under realistic communication conditions. Figure 3-3 illustrates the testbed.

The transmission simulation is hosted on an Opal-RT at Pacific Northwest National Lab (PNNL) while the distribution simulation is implemented on a separate Opal-RT at NC State. The distribution system model consists of three feeders represented by the IEEE 123 bus system which each have unique load and PV profiles and detailed load models at each node. A hardware inverter is hosted at UT Austin to represent one of the PV plants on distribution feeder 1. The rest of the PV plants are represented by detailed PV inverter models as in [22]. A VPN tunnel between NC State and PNNL allows for Modbus communication between the respective

controllers every 5 minutes to exchange distribution constraints and transmission adjustment requests. A Modbus connection between the distribution and transmission simulators allows for updates of the voltage and power flows at the interconnection point every minute. The communication connections are illustrated in Figure 3-4.

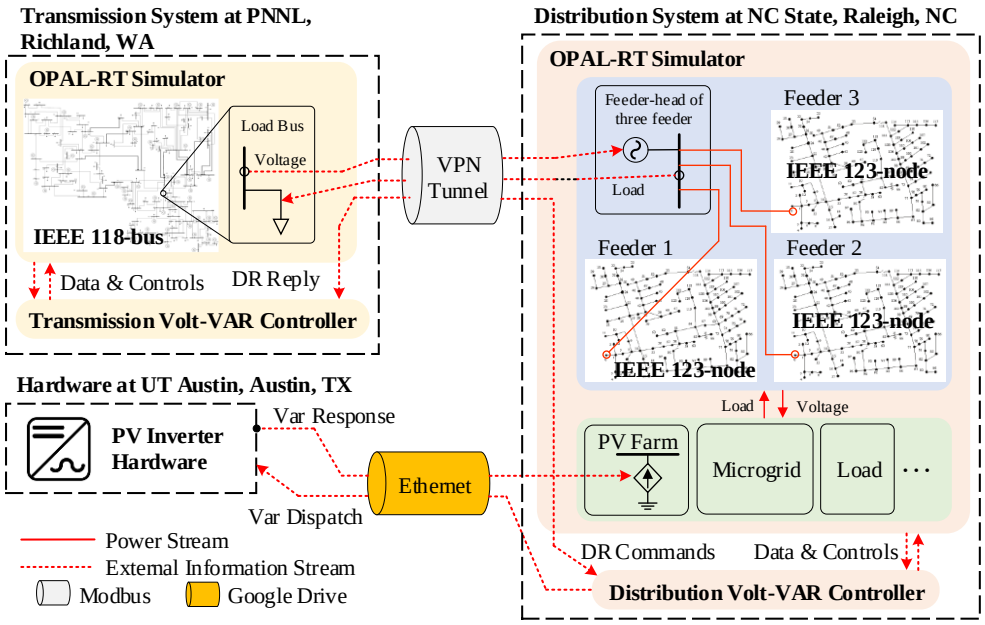

Figure 3-3. Networked HIL Testbed Setup

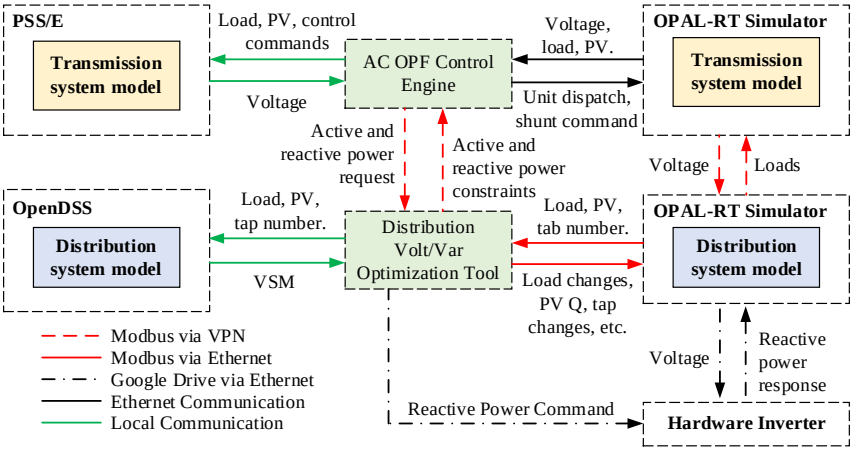

Figure 3-4. Networked HIL Testbed Communication Links

Real-time Test Results

Figure 3-5 shows how accurately the distribution system can respond to the transmission adjustment requests. The forecasted reactive power use by the distribution system with no control is shown for comparison. The results show that the actual reactive power use under CReST-VCT control matches closely with that requested by the transmission controller, which shows that the distribution system can effectively provide power changes to support transmission system needs.

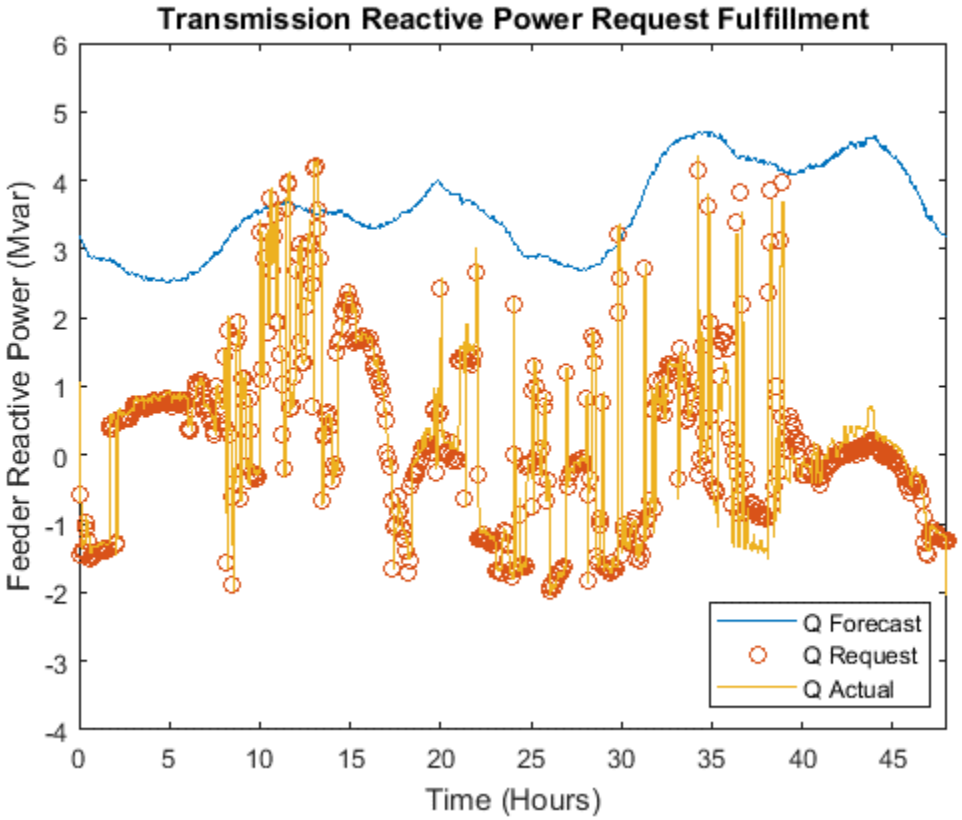

Figure 3-5. Reactive power adjustment fulfillment

Figure 3-6 shows the voltage results for two of the distribution feeders with CReST-VCT control. The voltages are well controlled on both feeders except for several hours when communication was lost between the distribution controller and the hardware inverter, which represents a PV plant on feeder 1. These results show that the distribution controller can

adequately control voltages while delivering reactive power adjustments for the transmission system. However, communication issues can have a major impact on the efficacy.

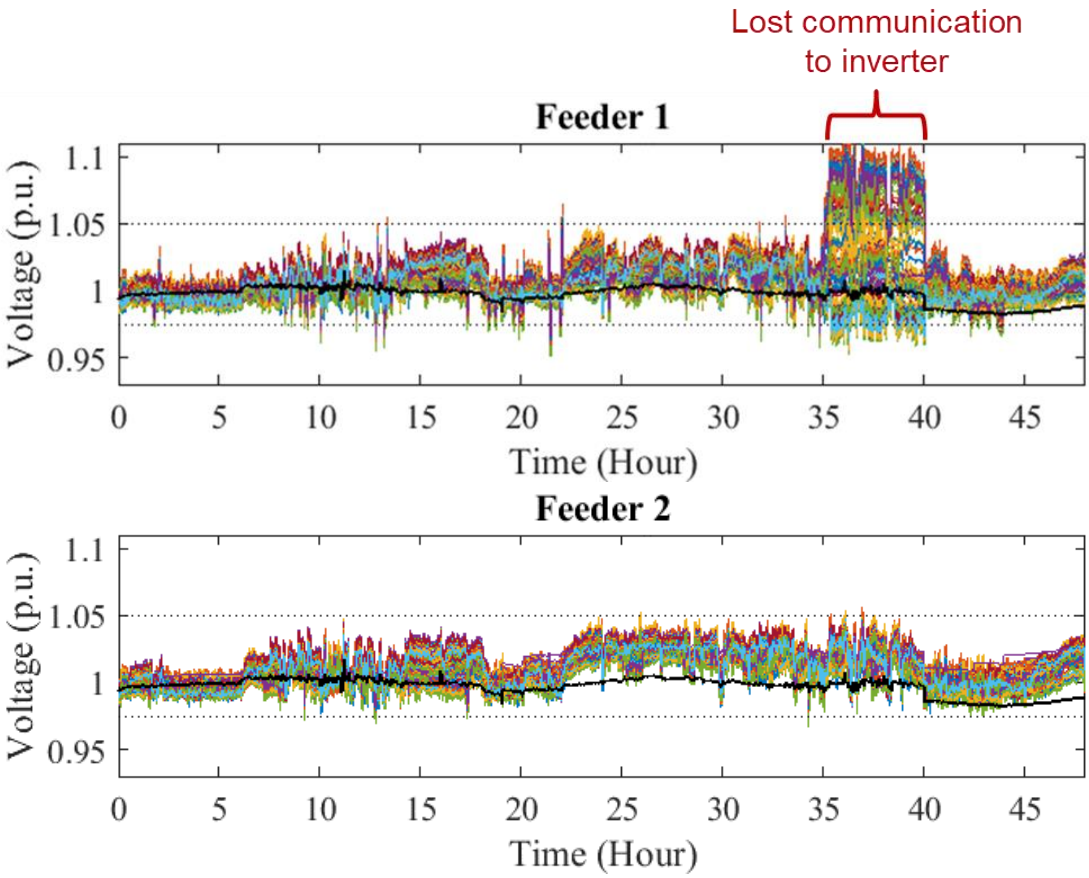

Figure 3-6. Distribution Feeder Node Voltages with CREST-VCT

Discussion and Future Work

This chapter illustrates how the CVVC can be successfully integrated with a transmission controller in order to provide coordinated control to the interconnection transmission and distribution systems. Real-time simulations show that the distribution controller can successfully meet voltage requirements while responding to transmission-side needs. Additional work is underway to mitigate the impacts of unreliable communication.

Chapter 4: **Chapter 4: A Regression-Based Voltage Estimation Method for Distribution Volt-Var Control with Limited Data**

Introduction

Inverter-based distributed energy resources (DERs), such as solar photovoltaic (PV) and battery energy storage systems, have superb controllability in terms of response accuracy and speed when regulating real and reactive power outputs. However, uncoordinated DER actions can cause a variety of operational issues. For example, when using smart inverters uncoordinatedly to provide local reactive power support for resolving voltage issues in distribution circuits with high PV penetrations, the number of switching operations of upstream or downstream voltage regulators can increase drastically, causing significantly wear-and-tear in those devices.

Thus, in recent years, coordinative volt-var control algorithms are proposed by researchers [8] - [9], [11]- [12], [14] and [15] for controlling smart inverters in DERs in coordination with voltage regulators (VRs) to replace the conventional volt-var control algorithms, which focus mainly on controlling utility-owned VRs using local measurements. Although the performance of those algorithms are satisfactory, there are two key drawbacks: an increasing demand on measurement data and communication bandwidth and control commands not compatible with the existing VR operation mechanism.

The first drawback arises because the voltage sensitivity calculations and centralized volt-var algorithms in [8] - [9], [11]- [12], and [14] rely on full visibility of nodal loads, voltages, PV outputs, and circuit parameters. However, distribution networks in reality have low visibility with only a few sensors located at the feeder head and possibly at controllable devices such as reclosers, PV plants, and voltage regulators. Visibility can be achieved through state

estimation algorithms, however conventional state estimations require online weighted-least-squares or similar optimization, which requires an online circuit model and can be computationally intensive, and often rely on pseudomeasurements which can introduce significant errors [23].

Data-driven, regression-based methods for estimating system operating conditions have been proposed in [15] and [24] - [26]. In [24], Weckx *et al.* proposed a method for calculating voltage sensitivity factors using historical smart meter data without relying on a circuit model. This approach requires full coverage with smart meter data for each feeder over at least one year, which may not be available. In [25], Deboever *et al.* proposed a multiple linear regression method trained on just nine power flow solutions to estimate the voltages throughout a distribution feeder with one large PV plant for any load and PV output combination. However, the authors didn't consider the impact of load diversity on voltage profiles. In [15] and [26], Zhang *et al.* and Rigoni *et al.* respectively proposed polynomial regressions on power flow results to predict voltages and sensitivity factors in a distributed manner based on measurements at each DER location. These distributed approaches require controllers at each DER location which can operate based on trained regressions. Regression-based approaches for centralized volt-var control schemes, where control decisions are made by a central controller with wider knowledge of the entire feeder state, have not yet been explored. Therefore, a computationally efficient and accurate voltage and voltage sensitivity estimation method that requires few real-time input data is needed for accurate, efficient, and cost-effective centralized volt-var control (CVVC).

The second drawback relates to the implementation of VR control actions. The volt-var control algorithms in [8], [12] and [14] calculate optimal tap changes and thus require

implementation of specific tap positions at each VR. However, conventional regulator controllers are not designed to implement specific tap positions; rather, a voltage set point, together with a predetermined voltage dead band, are used to determine the tap changer operation [27]. Thus, instead of sending a tap position, the VR control signal needs to be translated to a voltage set point.

To resolve those two issues, in this chapter, we propose *a machine learning based approach* for estimating voltages and voltage sensitivities online using measurements from a small number of sensors and *a mapping algorithm* for translating VR tap positions into voltage set points so the CVVC can be used with existing regulator controllers in the field. To prepare the offline training data for the regression-based estimator, a novel representative-scenario selection method is developed. The regression-based estimator predicts the node voltages at critical nodes using power measurements only at the feeder head and at the PV plant locations and estimates voltage sensitivities to control actions, including reactive power changes from DER inverters and VR tap changes. Trained offline, the estimator is effective on circuits with multiple large PV plants and VRs and diverse load profiles.

When used for online applications, the regression-based voltage and sensitivity estimators only require active and reactive power measurements at the feeder head and large PV plants. This will substantially reduce the need for extensive monitoring and communication infrastructure and reduces the computations needed to calculate the voltage sensitivities online. Limited online voltage measurements can optionally be used to improve the accuracy of the voltage estimator in the presence of load diversity and modeling errors.

To demonstrate the effectiveness of the proposed algorithm, we compare the regression-based method with the power flow based CVVC on a real, unbalanced distribution feeder.

Results show that the regression-based approach achieves adequate accuracy in CVVC with less communication needs and shorter computing time.

The main contributions of this chapter are summarized as follows: 1) a novel representative training scenario selection considering load diversity; 2) a critical-nodes based constrained volt-var optimization algorithm for reducing the computational speed, 3) a fast and accurate regression-based centralized voltage and voltage sensitivity estimation algorithm that is effective on large circuits with multiple large PV plants and VRs, 4) the online voltage estimation correction mechanism using limited voltage measurements, and 5) the tap-position-to-set-point mapping method for seamless implementation.

Method

The training and online application processes of the proposed regression-based volt-var controller is illustrated in Figure 4-1. There are two objectives in the offline training phase: minimize the measurement and communication infrastructure needs by only collecting data from a limited number of existing sensors and accelerate the computation speed so optimization can be achieved inside each control interval.

To achieve the two objectives, it is necessary to use a regression-based estimator for predicting nodal voltage and voltage sensitivity. The estimator is trained with results from offline power flow cases using historical data. In this chapter, we propose a centralized method which only requires regressions housed in one central controller. We introduce representative scenario selection and voltage correction to address load diversity and the tap-position-to-set-point mapping to implement VR actions.

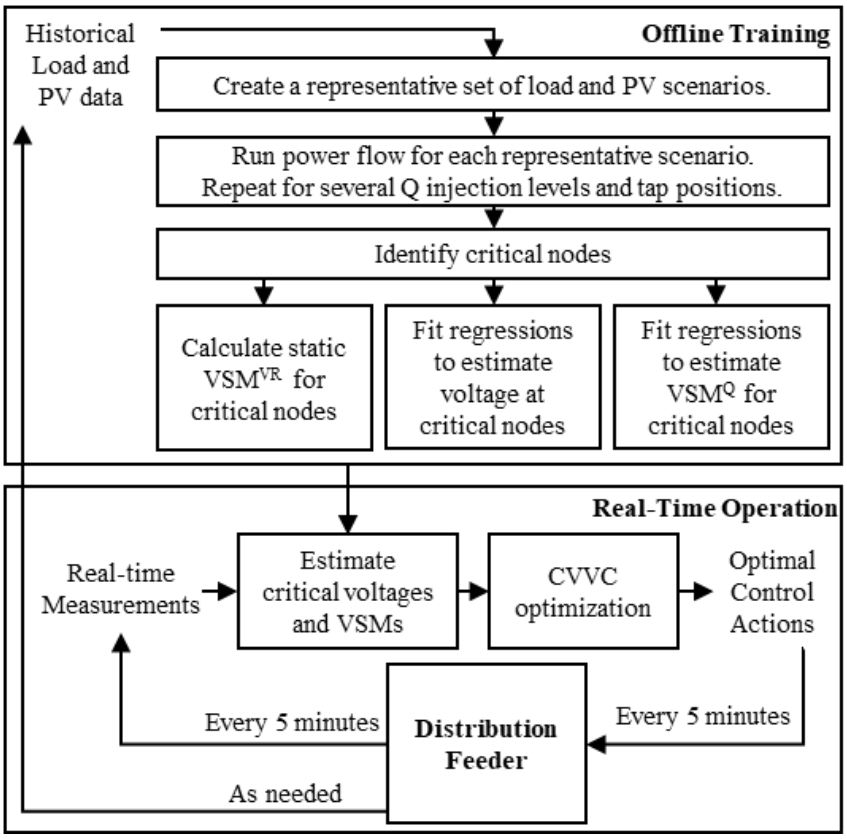

Figure 4-1. Flowchart of the offline training and online operation processes

Representative Scenario Selection

As a first step, collect one year of historical smart meter data for a distribution feeder. If smart meter data is not available, the disaggregation algorithm in [13] can be used to create diverse synthetic smart meter data for each load node. Then, plot the feeder head load, P_{feeder}, versus the total PV power output, P_{PVTOT} on a scatter plot and divide into blocks, as shown in Figure 4-2. For each scenario, calculate the load and PV centers, D_L and D_{PV} as

$$D_L = \frac{1}{\sum_{i \in N} L_i} \sum_{i \in N} D_i \times L_i \quad (1)$$

$$D_{PV} = \frac{1}{\sum_{i \in N} P_i} \sum_{i \in N} D_i \times P_i \quad (2)$$

where D_i is the electrical distance of node i from the feeder head; L_i and P_i are the load and PV injection at node i, respectively. Note that the load and PV centers provide a measure of how the load and PV injections are distributed throughout the feeder.

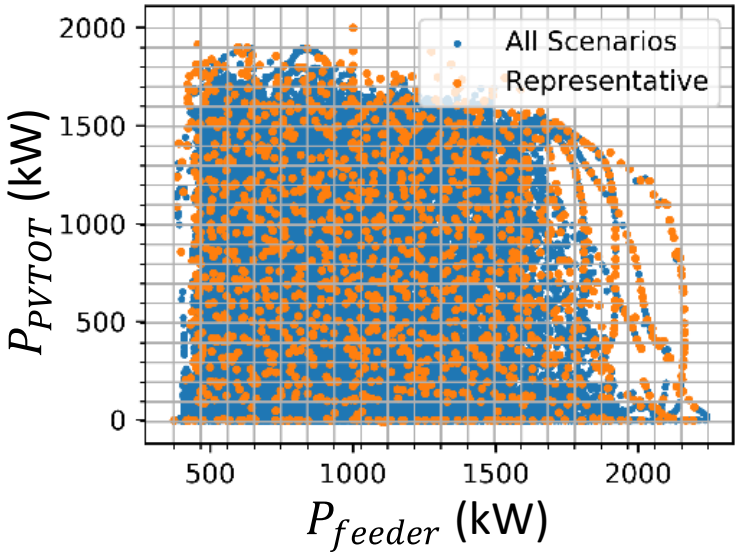

Figure 4-2. Selection of typical operation scenarios

Next, choose 6 scenarios (i.e., maximum, median, and minimum load and PV centers shown by the orange dots) from each block. These scenarios will represent all the scenarios with similar P_{feeder} and P_{PVTOT} levels and are chosen because they represent the cases where the maximum, minimum, and median voltages are expected based on the load and PV distributions, as shown in Figure 4-3. By choosing these specific scenarios from each block, the key variations of scenarios can be captured to reduce the overall bias in the training data.

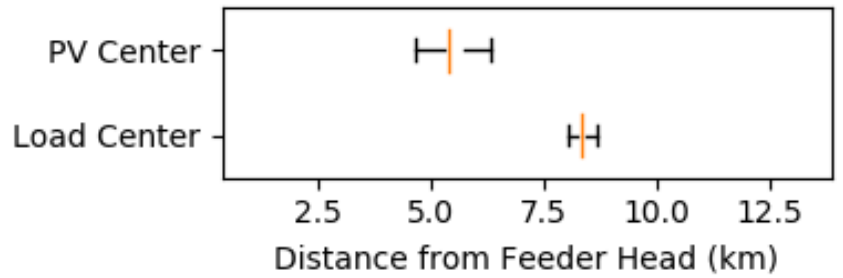

(a)

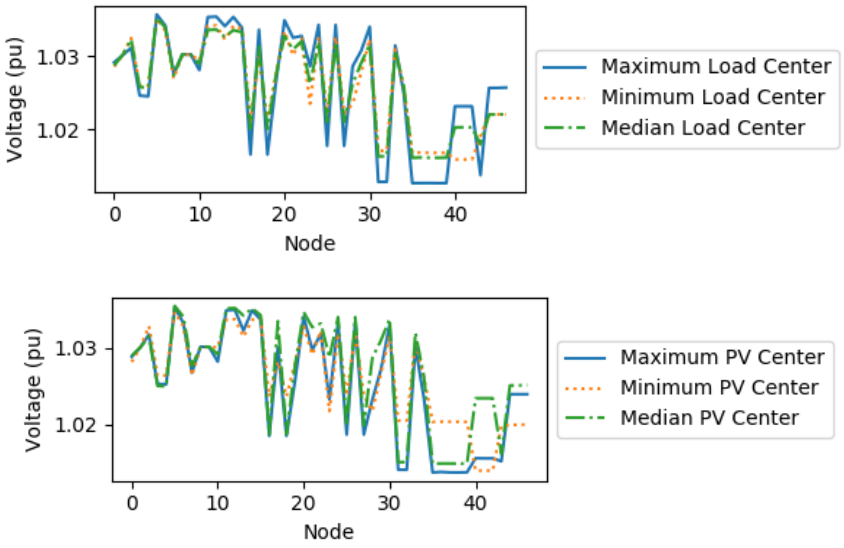

(b)

Figure 4-3. (a) Minimum, maximum, and median load centers for one load/PV block and (b) resulting voltage profiles

Training Data Preparation

The training data generation process is detailed in algorithm 1. For the first selected representative scenario, perturb each regulator's tap up/down and run power flow to establish the relationship between the tap changes and nodal voltage variations. Then, for each selected representative scenario, set the reactive power injection at each PV plant at different levels and run power flow for each case to establish the relationship between PV reactive power injection/absorption and nodal voltage variations.

Algorithm 1: Training Data Generation

```
Select representative scenarios
Solve power flow for the first scenario (no PV reactive power injection and no VR actions)
for each voltage regulator
  Increase the tap position by 1
  Record the voltage change
  Return the tap to the initial position
for each scenario
  for each PV plant
    for each Q value in (-100%,-80%...100%)
      if Q is within the PV excess capacity
        Set PV reactive power to Q
        Solve power flow
        Record Voltages and Power measurements
      else
        Skip to next Q value
      end
    end
    revert PV reactive power to 0
  end
end
```

Critical Nodes Selection

In practice, the CVVC optimization problem is constrained by nodes with extreme voltages. Therefore, we define critical nodes as the nodes where the highest or lowest voltages on the feeder are most likely to occur. Thus, by narrowing the consideration from all nodes to only the critical nodes, we can simplify the CVVC optimization problem significantly.

As shown in Figure 4-4, the initially selected critical nodes include the feeder head node, the primary and secondary nodes of each voltage regulator and the PV plant locations where voltage rise can cause extreme voltages. Then, after each scenario run, any node with the highest or lowest voltage will be added to the critical node list. Note that such nodes usually occur near the ends of the feeder.

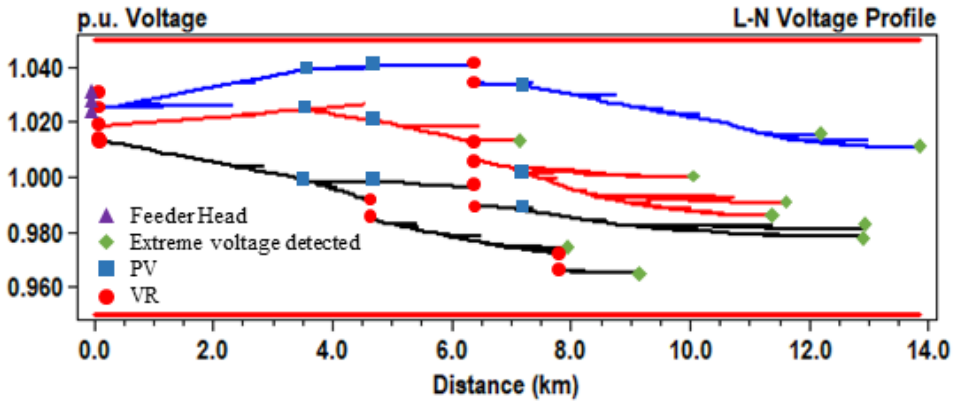

Figure 4-4. Voltage profile with critical nodes

Estimating voltage only at the critical nodes ensures that the online optimization will be able to address the most extreme voltage violations without considering voltage constraints at every node in a large system. This can also reduce the number of regressions that are needed as part of the estimator, as each node considered requires one regression for voltage estimation and one regression for voltage sensitivity estimation.

Voltage Estimator and Voltage Sensitivity Estimator

Linear regression is used in the voltage estimator to calculate voltage from active and reactive power measurements on each phase at the feeder head and at each PV plant. Least squares regression is used to fit the power flow nodal voltages with respect to the power measurements. The voltage-sensitivity estimator estimates the voltage sensitivities with respect to PV reactive power injections/absorptions for each scenario using power flow results. For each power flow result, after the PV reactive power for one plant is perturbed, the voltage values are subtracted from the voltage values of the previous power flow result. The voltage sensitivity is the change in voltage divided by the change in reactive power. The voltage sensitivities are calculated for each critical node with respect to each PV plant across all power flow results.

Figure 4-5shows the voltage sensitivity, δ^Q, for one critical node with respect to one PV plant and how it changes with respect to various possible feeder measurements. The trends with respect to voltages at the PV node, voltages at the critical node being considered, active and reactive power at the feeder head, and active and reactive power at the PV plant are shown. The voltage sensitivity shows a clear trend with respect to the reactive power at the feeder head. Therefore, the reactive power measured at the feeder head is the sole variable used to regress the voltage sensitivity on. Based on the inverse shape of the curve, δ^Q can be fit by a curve using reactive power at the feeder head, Q_s, for each critical node and PV plant pair as

$$\delta^Q = a/(3000 + Q_s)^b \quad (3)$$

The resulting curve and residuals for one critical node with respect to one PV plant are shown in Figure 4-6.

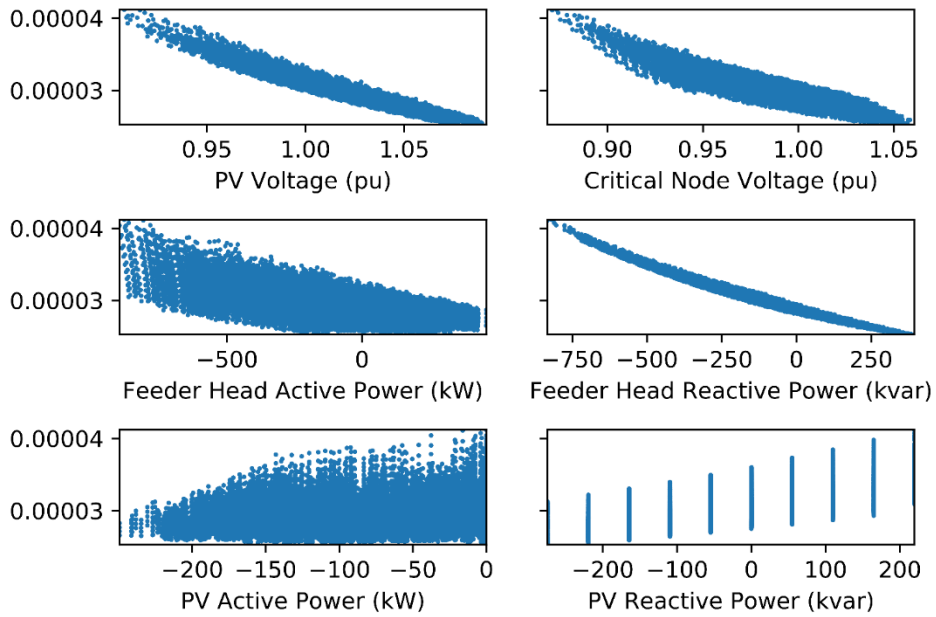

Figure 4-5. δ^Q variation with respect to other measurements

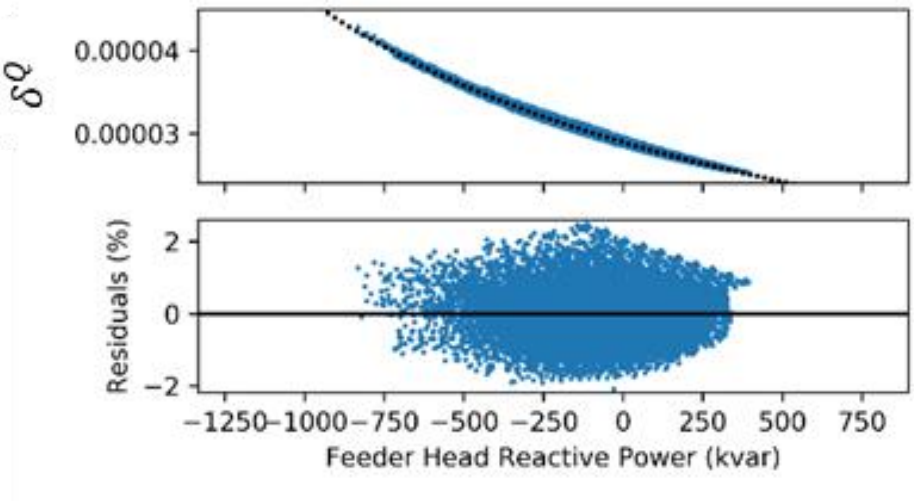

Figure 4-6. δ^Q with curve fit and residuals

The voltage-sensitivity estimator also accounts for the impact of tap changes on voltage variations. Because the voltage sensitivity with respect to tap changes does not vary significantly across different scenarios, the voltage change caused by a tap change is only calculated for one scenario and ignoring the reactive power injection/absorption from the PV plants. The voltage sensitivity, $\delta_{i,r}^{VR}$, is calculated as

$$\delta_{i,r}^{VR} = V_i^r - V_i^0 \quad \forall r \in R, \forall i \in N \tag{4}$$

where V_i^r is the voltage at node i after a single tap change on regulator r and V_i^0 is the voltage before the tap change.

Online Operation

For online operation, we first use the regression models along with limited measurements to calculate the critical voltages and sensitivities. Then, those values are input to the CVVC optimization to determine the optimal control actions.

Voltage Estimation

The voltage at each critical node is calculated as

$$\hat{V}_i = \sum_{m \in M} \alpha_{m,i} m + \sum_{r \in R} \delta_{i,r}^{VR} (T_r^t - T_r^0) \quad (5)$$

where M is the set of available active and reactive power measurements at the feeder head and PV plant locations and $\alpha_{m,i}$ represents the corresponding regression coefficients for estimating voltage at node i. The first term of equation (5) estimates the voltage at node i assuming the regulators are each on the same tap as they were during the initial training power flows. The second term superimposes the voltage change caused by the difference in regulator tap positions compared to those used in the training power flows using the voltage sensitivity calculated by (4). Thus, the CVVC controller can determine the voltages at all critical nodes using (5) with only active and reactive power measurements at the feeder head and PV plant locations and the current tap positions of each regulator.

Next, the voltage sensitivities are calculated based on the reactive power measurement at the substation and the fitted δ^Q curves. The δ^Q values are calculated for each critical node and for each PV plant. The critical node voltages and voltage sensitivities are input into the CVVC optimization along with the PV and VR device constraints.

Voltage Estimation Correction

Voltage estimation error,ε_r, is introduced because nodal voltages will vary when loads and PVs are distributed differently throughout the feeder. The use of static $\delta_{i,r}^{VR}$ values will also introduce a small error in calculating nodal voltage changes. Voltage measurements at the secondary bus of voltage regulator, V_r, are normally used in conventional local regulator control. Therefore, ε_r is calculated as

$$\varepsilon_r = V_r - \hat{V}_r \quad \forall r \in R \tag{6}$$

where $\hat{V}_r$ is the estimated voltage at the secondary bus of each voltage regulator. Thus, (5) becomes

$$\hat{V}_i = \sum_{m \in M} \alpha_{m,i} m + \sum_{r \in R} \delta_{i,r}^{VR} (T_r^t - T_r^0) + \varepsilon_{r_i} \tag{7}$$

where r_i is the regulator immediately upstream of node i. Thus, we assume that voltages downstream of a regulator will have similar voltage estimation errors as the regulator bus due to their close electrical connection as illustrated in Figure 4-7.

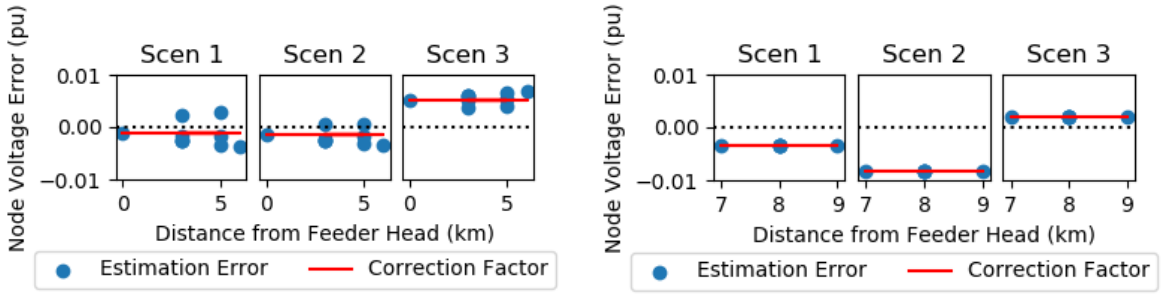

Figure 4-7. Voltage error and correction factor, ε_r, for nodes downstream of two VRs for 3 different scenarios

Algorithm 2: Voltage Estimation with Measurement Correction
1: Measure real and reactive power at feeder head and PV plants
2: Measure voltage at each regulator secondary, V_r
3: Estimate voltages at each regulator secondary, $\hat{V}_r$, using (5)
4: Calculate correction factor, ε_r, using (6)
5: Estimate voltage at each critical node using (7)

Command Implementation

Once the optimal commands are decided, the reactive power set points can be sent directly to the smart inverters to be implemented. For voltage regulator commands, the optimal tap positions cannot be implemented directly using conventional regulator controllers. Conventional regulator controllers operate based on a voltage set point, V_T, with a dead band, B,

and time delay. Therefore, the desired tap position, T, needs to be translated into V_T, which can be implemented by the regulator controller by

$$V_T = \begin{cases} V_s^1 + \left(\frac{1}{2}\mathrm{B} - \frac{1}{2}\mathrm{T}\right) & \text{if } dT > 0 \\ V_s^1 - \left(\frac{1}{2}\mathrm{B} - \frac{1}{2}\mathrm{T}\right) & \text{if } dT < 0 \\ V_s^1 & \text{if } dT = 0 \end{cases} \quad (8)$$

If no tap change is needed, the set point is set to the expected voltage at the regulator's secondary bus, V_s^1, after all other control action are implemented, which is calculated using the voltage sensitivities. This ensures that the regulator will be at the center of its band when the command is implemented and there will be no tap changes unless a voltage change with magnitude at least half of the VR's band occurs. If a tap change is needed, the set point is chosen such that the desired tap position will be the first tap within the regulator's new band. This forces the regulator to change taps appropriately to reach the new band.

Implementing tap changes by adjusting the local regulator set point achieves three benefits. First, the existing local regulator controller can be used to implement centrally optimized commands. Second, the local regulator control can operate to prevent over-voltages and under-voltages that may occur if the voltage continues to increase or decrease throughout the control interval. Finally, if there is some error in the voltage estimate, using the local controller to achieve a desired voltage set point ensures that the nodes near the regulator secondary will achieve the expected voltage despite estimation errors.

Optimization Formulation

The CVVC optimization determines the best combination of reactive power control at each PV plant and tap changes for each regulator. Therefore, the decision variables are the

change in tap position up ΔT_r^+ or down , ΔT_r^- for each regulator $r \in R$ and reactive power injection Q_k^+ and absorption Q_k^- by each PV plant $k \in$ K.

The CVVC problem is formulated as

$$\min \ (\sum C_r(\Delta T_r^+, \Delta T_r^-) + \sum C_k(Q_k^+, Q_k^-)) \quad (9)$$

$$\underline{Q_k} < Q_k^+ - Q_k^- < \overline{Q_k} \qquad \forall k \in K \quad (10)$$

$$\underline{T_r} < T_r + \Delta T_r^+ - \Delta T_r^- < \overline{T_r} \quad \forall r \in R \quad (11)$$

$$\Delta T_r^+ + \Delta T_r^- < \overline{\Delta T} \qquad \forall r \in R \quad (12)$$

$$\underline{V} < V_i^0 + (Q_k^+ - Qk— Q_k^0) \times \delta_{i,k}^Q + (\Delta T_r^+ - \Delta T_r^-) \times \delta_{i,r}^{VR} < \bar{V} \qquad \forall i \in N \quad (13)$$

$$C_r(\Delta T_r^+, \Delta T_r^-) = c_r \times (\Delta T_r^+ + \Delta T_r^-) \qquad \forall r \in R \quad (14)$$

$$C_k(Q_k^+, Q_k^-) = c_k \times (Q_k^+ + Q_k^-) \qquad \forall i \in I \quad (15)$$

The objective of the CVVC optimization is to minimize the cost of control actions. (10) gives the reactive power constraints for each PV plant considering the total capacity and the current active power output. (11) constrains the resulting tap position within the voltage regulator's limits. (12) limits each voltage regulator to a reasonable number of tap changes for each 5-minute control interval. (13) enforces the voltage constraints at each critical node, using the voltage sensitivity matrices to calculate the expected voltages after control actions are implemented. (14) and (15) give the cost functions for tap changes and PV reactive power, respectively. Note that the cost functions are simply flat rates for each tap change and each kvar of reactive power injected or absorbed.

In some cases, the voltages cannot be fully corrected by the available resources. Therefore, an additional set of decision variables V_i^{vio} is added for each critical node $i \in N$ to allow small voltage violations. The voltage constraint in (13) is replaced by (16) which allows for controlled voltage violations at each node. An updated objective function given by (17) uses

the sum of squares of V_i^{vio} as a penalty in the objective. The optimization is solved first with equations (9) through (15) to enforce all voltage constraints.

In cases where the problem is infeasible, the controller will minimize the sum of squared voltage violations instead of enforcing voltage constraints. So (9) is replaced by

$$\min \ \alpha \times (\sum C_r(\Delta T_r^+, \Delta T_r^-) + \sum C_k(Q_k^+, Q_k^-)) + \beta \times \sum_N {V_i^{vio}}^2 \quad (16)$$

$$\underline{V} - V_i^{vio} < V_i^0 + (Q_k^+ - Qk — Q_k^0) \times \delta_{i,k}^Q +$$

$$(\Delta T_r^+ - \Delta T_r^-) \times \delta_{i,r}^{VR} < \bar{V} + V_n^{vio} \qquad \forall i \in N \quad (17)$$

Simulation Results

Test Feeders and Data Sets

The estimator is tested in conjunction with the CVVC on a real, unbalanced rural circuit. The rural circuit has 1003 buses (1284 single-phase nodes) and includes 2 three-phase regulators and 2 single-phase regulators. There are 3 PV plants added to each circuit to give a total PV penetration equal to 100% of peak load as shown in Figure 4-8. One-year, one-minute resolution load profiles for each load node were allocated using the algorithm presented in [13] to account for load diversity. One-year, one-minute resolution PV profiles are taken from Pecan street data [14] and scaled so the peak PV output matches the PV capacity for each plant.

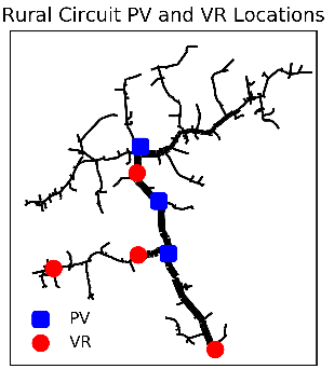

Figure 4-8. Test feeder map with PV and VR locations

Case Setup

To assess the efficacy of the proposed methods, four cases are compared as summarized in Table 4.1.

Table 4.1. Simulation Case Setup

Case	Voltages Used	Voltages	Voltage Sensitivities	VR control
A	All Nodes	Measured	Perturbation	Tap positions
B	Critical Nodes	Estimator	Estimator	Tap positions
C	Critical Nodes	Estimator	Estimator	Set points
D	Critical Nodes	Estimator/correction	Estimator	Set points

In case A, the CVVC is run assuming the controller has full visibility of the entire feeder. Every 5 minutes, the voltage inputs are taken directly from power flow results. The voltage sensitivities are calculated at each time step using the perturbation method as in [8]. The optimization formulation is the same as discussed above, except that, in the full visibility case, the voltage constraints are considered at every node instead of only critical nodes. The resulting optimal control actions are implemented for the next 5 minutes of simulation, and tap positions are implemented directly without translation to voltage set points.

In case B, the CVVC controller will use the critical-nodes based volt-var optimization algorithm to determine the optimal tap changes for voltage regulators. Voltages at the critical nodes are estimated by voltage and voltage sensitivity estimators with no measurement correction. The one-year load and PV profiles are used as the basis for creating the representative scenarios. The estimator is trained according to the previous sections. Every 5 minutes, the power measurements are taken and used to estimate the critical node voltages and sensitivities. Those values are input into the CVVC optimization and the actions are implemented as in case A.

Case C builds on case B but instead of implementing tap positions directly, the optimal tap changes are translated into voltage set points. Each regulator is given a bandwidth of 4V on a 120V base.

Case D builds on case C but with voltage correction implemented using measurements at each VR secondary bus. Additional simulations were run to illustrate the impact of different bandwidths for cases C and D.

For each case, the circuit is simulated in OpenDSS for 4 months (i.e., 1 month in each season) at one-minute resolution. For all cases, the voltage limits in the optimization were set to (0.975,1.04) to provide a 0.01 margin for error within the actual desired limits of (0.965,1.05).

Efficacy of Representative Scenario Selection

The proposed PV-Load-center based representative scenario selection method is compared to the random selection approach, in which six scenarios are selected randomly from each load and PV block.

The voltage estimator is first trained on the rural circuit and then used to estimate voltages throughout the winter month. As shown in Figure 4-9, the guided selection method reduces the bias in voltage estimates by ensuring that the full range of load and PV distributions is considered. With random selection, more common load and PV distributions are more likely to be selected which leads to bias and higher error in less common scenarios.

47 critical nodes are selected as shown in Figure 4-10, representing 3.7% of all nodes. In addition to the PV, VR, and feeder head nodes, the extreme voltage nodes all occur at or near the ends of feeder branches.

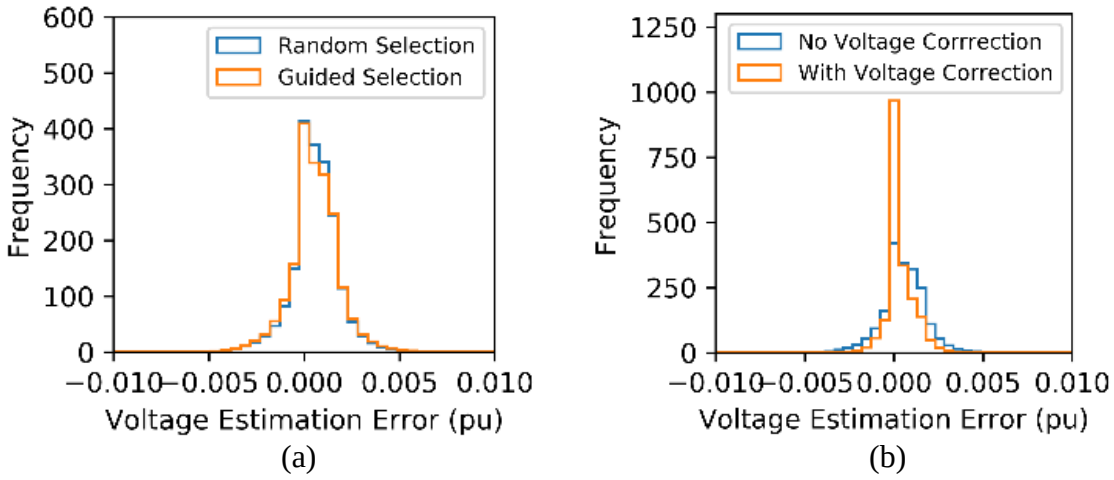

Figure 4-9. Voltage estimation error with (a) random and guided selection and (b) with and without voltage correction

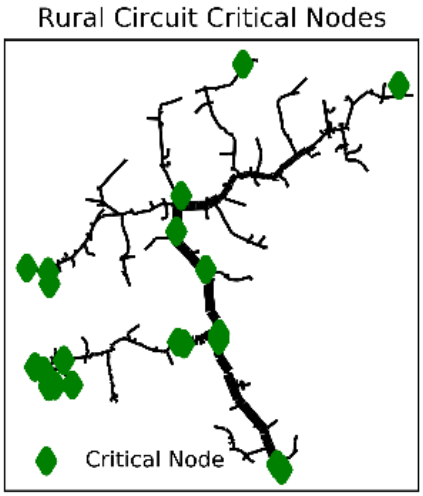

Figure 4-10. Test Feeder with Critical Node Locations

Efficacy of Voltage Measurement Correction

In Figure 4-9, we compared voltage estimation errors for cases with and without voltage correction (i.e., using VR secondary voltage measurements for voltage correction) by running the rural circuit model for one month in winter. For both methods, voltage estimation errors are within [-0.01, 0.01] p.u., which is adequate for volt-var control. However, the estimates are much more accurate with less bias when voltage estimation errors are corrected by measurements.

Overall Performance Comparison

Six performance metrics are used to quantitatively compare the performance of the four CVVC algorithms. To compare the voltage regulation effects, we compute the maximum voltage violation magnitude (MVVM) and the number of voltage violations (NVV) based on 10-minute rolling average voltage measurements at every node in the system. To compare the control resource usage, we calculate the number of tap changes (NTC), the reactive power (Q) cost, the tap change (T) cost, and total cost for each month of control. Table 4.2 summarizes the simulation results.

Table 4.2. Rural Circuit Results Summary

Season	Case	MVVM	NVV	NTC	Q Cost	T Cost	Total Cost
Winter month	A	0.0072	39	411	694.30	57.54	751.84
	B	0.0007	43	456	605.19	63.84	669.03
	C	0	0	514	582.62	71.96	654.98
	D	0	0	665	591.61	93.10	684.71
Spring month	A	0	0	39	361.32	5.46	366.78
	B	0	0	21	451.24	2.94	454.18
	C	0	0	72	535.55	10.08	545.63
	D	0	0	77	482.08	10.78	492.86
Summer month	A	0	0	266	562.31	37.24	599.55
	B	0	0	251	513.52	35.14	548.66
	C	0.0007	98	437	552.23	61.18	613.41
	D	0	0	449	527.34	62.86	590.20
Fall month	A	0	0	11	269.27	1.54	270.81
	B	0	0	18	154.66	2.52	157.18
	C	0	0	37	221.31	6.44	227.75
	D	0	0	51	253.15	7.14	260.29

Impact of Voltage Estimation and Use of Critical Nodes

Performance indicators match closely between cases A and B in all seasons, which shows that the estimator can provide adequate voltage visibility and sensitivity estimates to the CVVC to provide a similar level of voltage control at similar cost compared to a system with full visibility. Using only critical nodes in the optimization does not lead to voltage violations at unmonitored nodes in these cases.

Impact of VR set points

The use of VR set points rather than tap positions in cases C and D invariably increases the total number of tap changes. However, this change is necessary to implement VR actions using existing VR controllers. The addition of local control by VRs through the use of set points also eliminates the small number of voltage violations observed in the winter month in cases A and B. Those violations occur due to voltage changes within a control interval, and can be corrected by the VR's local control.

Impact of voltage correction

The addition of voltage correction in case D eliminates the 98 voltage violations observed in the summer month in case C. In all cases, the addition of voltage corrections in case D brings the total control cost closer to the observed value with full visibility in case A.

Impact of Voltage Regulator Dead Band Settings

Table 4.3 compares the results with different VR dead bands for cases C and D on the rural circuit. Increasing the VR bandwidth is one way to reduce the number of unnecessary tap changes when local control is used [27]. The results in table III show that this holds true when centrally optimized VR voltage set points are used. When the bandwidth is reduced to 2V,

excessive tap changes are observed. In addition, voltage violations become common because the VRs tend to operate on small local voltage fluctuations to the detriment of the overall system.

Table 4.3. Summary of VR Bandwidth Impacts on the Rural Circuit in Winter

Regulator Dead Band	Case	MVVM	NVV	NTC	Q Cost	T Cost	Total Cost
4V	C	0	0	514	582.62	71.96	654.98
	D	0	0	665	591.61	93.10	684.71
3V	C	0	0	650	597.14	91.00	688.14
	D	0.0009	29	710	600.60	99.40	700.00
2V	C	0.0047	172	1445	875.59	202.30	1077.90
	D	0.0048	241	1354	980.43	189.56	1169.99

Comparison between Case A and Case D

We compare the performance of the proposed regression-based method for estimating voltages and voltage sensitivities for volt-var control with voltage correction with the CVVC with full visibility, where real and reactive power measurements of all nodes are used. The nodal voltage magnitudes, reactive power injections, and tap positions for cases A and D for the rural circuit in winter are compared in Figure 4-11, Figure 4-12, and Figure 4-13, respectively. Tables V and VI summarize the actions taken by each PV and VR, respectively.

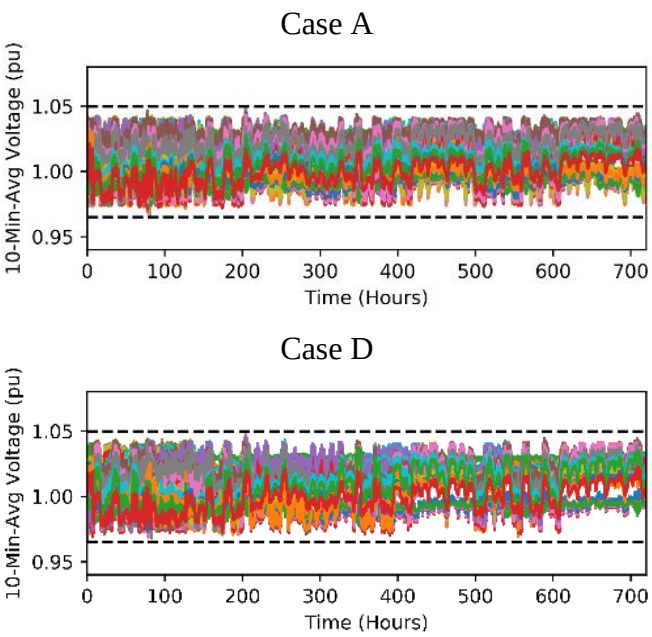

Figure 4-11. 10-minute average voltage results on the rural curcuit in winter

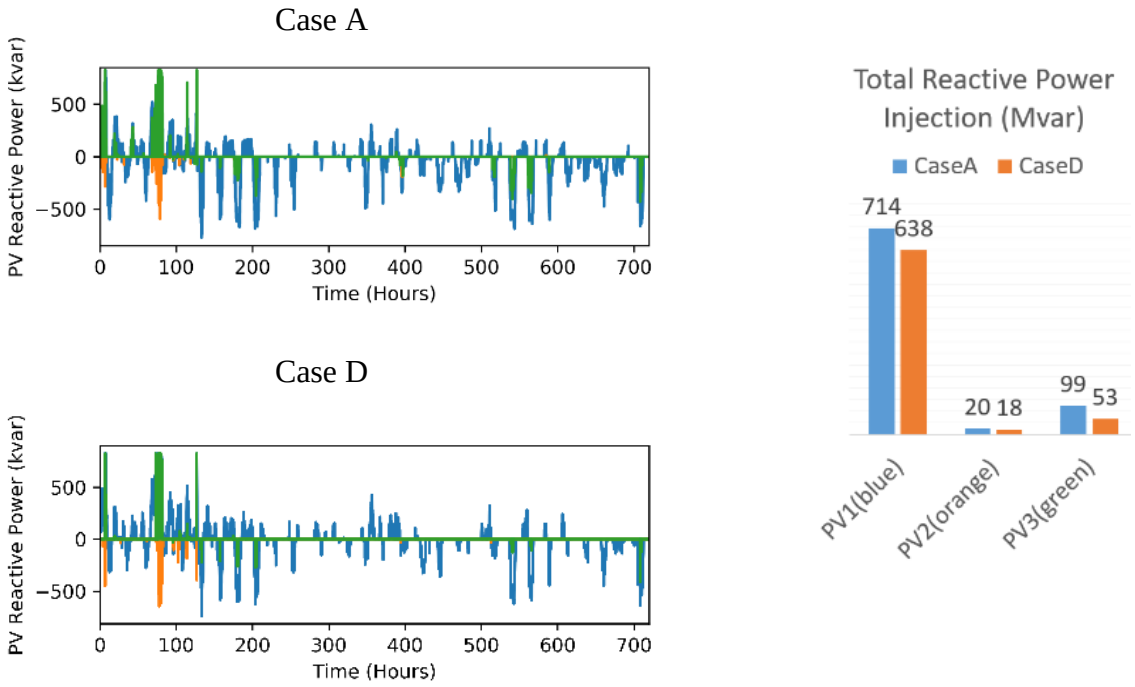

Figure 4-12. Reactive power injections by each PV plant on the rural circuit in winter

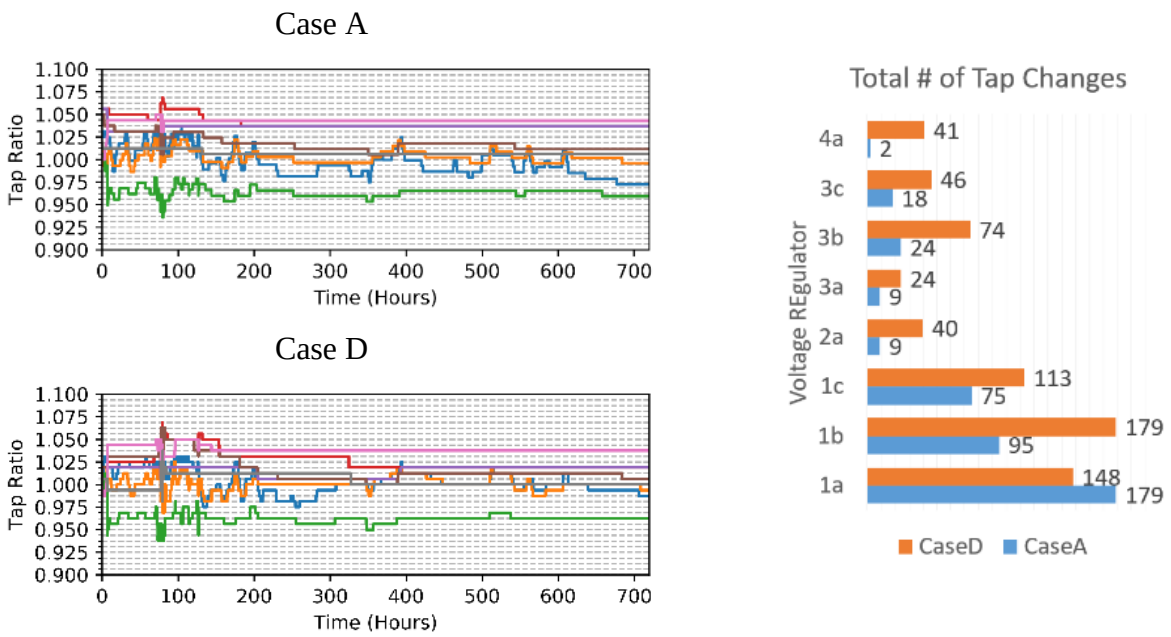

Figure 4-13. Tap positions and number of tap changes for each VR on the rural circuit in winter

For both approaches, the nodal voltages remain within the desired limits in nearly all cases. Reactive power control at each PV plant is very similar between the two cases, which shows that the CVVC can accurately assign reactive power commands to the most effective PV plants based on the estimated voltages and sensitivities using measurements from only the feeder head and the PV sites corrected by measurements from voltage regulators.

The tap positions for each regulator are similar under both CVVC control schemes. The number of tap changes increases for nearly all regulators in case D compared to case A. These are mainly triggered by the local regulator controller between optimizations.

Speed Comparison

The computational time needed to calculate the optimal control actions every 5 minutes is compared in Figure 4-14. For the proposed method (case D), … The computational time is reduced mainly through the elimination of the online perturb-and-observe voltage sensitivity calculation and the reduction of optimization voltage constraints to only include critical nodes.

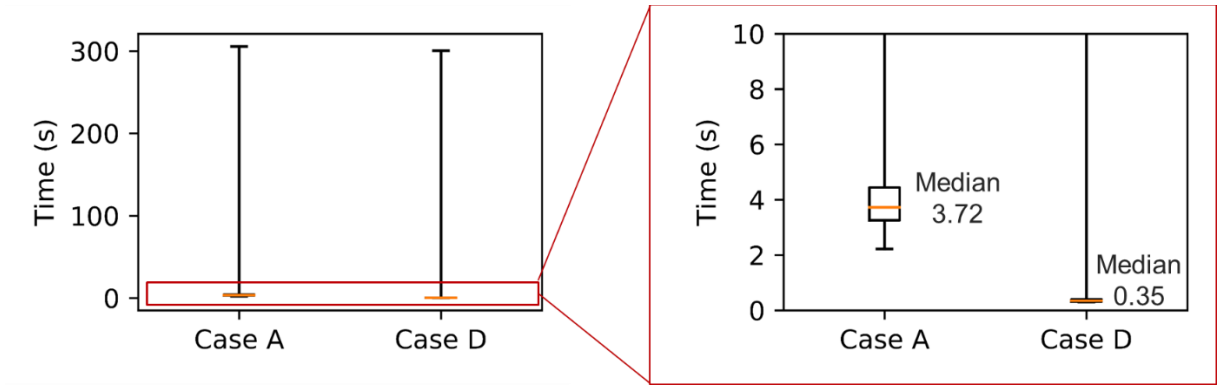

Figure 4-14. Computational speed comparison Boxplot

Conclusion

This chapter addresses several practical challenges of implementing CVVC on distribution feeders. First, a method to estimate voltages and voltage sensitivities online using regressions on offline power flow results is presented. The estimator provides visibility of the critical node voltages across the distribution feeder using only active and reactive power measurements at the substation and at each PV plant. This estimator provides the real-time data needed to run a centralized volt-var control algorithm using very limited communication infrastructure, which greatly reduces the capital needed to implement a centralized volt-var control system. By identifying critical nodes, the number of constraints is greatly reduced compared to the full visibility case, which improves online computational time. Finally, the implementation of optimal tap positions using conventional regulator control equipment is addressed. The proposed method is effective on large circuits with diverse loads and multiple large PV plants with diverse output profiles.

This method assumes an accurate circuit model, reliable measurements, and reliable communication to the feeder head and PV plants. The voltage correction mechanism proposed here can mitigate some impacts of modeling and measurement errors. However, additional work

is needed to understand the robustness of this method to circuit modeling errors, measurement errors and communication failures.

Chapter 5: **Summary and Future Work**

This dissertation details the development of a centralized distribution volt-var control scheme which coordinates PV plants with traditional utility-owned voltage regulation devices. This method uses real-time measurements and an accurate voltage sensitivity matrix as inputs to a mixed-integer nonlinear program which optimizes control actions to minimize cost and ensure voltage and device constraints are met. In chapter two, the algorithm is laid out in its theoretical form and tested with both software and real-time simulations. With full visibility and plentiful computational power, the algorithm is successful in its theoretical form. In chapter three, the CVVC is integrated with a transmission controller to provide voltage support to the transmission system. In chapter four, the algorithm improved to address the practical considerations of limited visibility, limited computational power on grid-edge devices, and legacy device controllers. The proposed method is effective on large circuits with diverse loads and multiple large PV plants with diverse output profiles.

By addressing practical concerns at the forefront of distribution operation in the face of continuing increases in PV penetration, this paper provides a step toward a feasible solution to the centralized volt-var control problem for circuits with both traditional voltage regulation devices and high PV penetration. Some practical considerations remain. The current method assumes an accurate circuit model, reliable measurements, and reliable communication to the feeder head and PV plants. Simulations in chapter three show that unreliable communication can have significant impacts on the efficacy of the CVVC. The voltage correction mechanism proposed in chapter 4 may mitigate some impacts of modeling and measurement errors. However, additional work is needed to understand and improve the robustness of the improved method to circuit modeling errors, measurement errors and communication failures.

REFERENCES

[1] ANSI C84.1: American National Standard for Electric Power Systems and Equipment Voltage Ratings (60 Hertz). NEMA, 2016.

[2] J. J. Grainger and S. Civanlar, "Volt/var control on distribution systems with lateral branches using shunt capacitors and voltage regulators part I: the overall problem," IEEE Transactions on Power Apparatus and Systems, Vols. PAS-104, no. 11, pp. 3278-383, 1985.

[3] "State Solar Spotlight: North Carolina," solar Energy Industries Association, 2020.

[4] "State Solar Spotlight: California," Solar Energy Industries Association, 2020.

[5] W. Ren and H. Ghassempouraghamolki, "Tuning of Voltage Regulator Control in Distribution," in IEEE Power and Energy Society General Meeting, Portland, 2018.

[6] "IEEE Standard for Interconnection and Interoperability of Distributed Energy Resources with Associated Electric Power Systems Interfaces," IEEE 1547-2018, 2018.

[7] Stochastic Analysis to Determine Feeder Hosting Capacity for Distributed solar PV, Palo Alto, CA: EPRI, 2012.

[8] C. McEntee, D. Mulcahy, J. Wang, X. Zhu and N. Lu, "A VSM-Based DER Dispatch MINLP for Volt-VAR Control in Unbalanced Power Distribution Systems," in IEEE Power & Energy Society General Meeting, Atlanta, GA, 2019.

[9] X. Zhu, J. Wang, D. Mulcahy, D. L. Lubkeman, N. Lu, N. Samaan and R. Huang, "Voltage-Load Sensitivity Matrix Based Demand Response for voltage Control in High solar Penetration Distribution Feeder," in IEEE Power & Energy Society General Meeting, Chicago, 2017.

[10] S. Conti, S. Raiti and G. Vagliasindi, "Voltage sensitivity analysis in radial MV distribution networks using constant current models," in IEEE International Symposium on Industrial Electronics, Bari, Italy, 2010.

[11] Q. Zhou and J. W. Bialek, "Simplified Calculation of Voltage and Loss Sensitivity Factors in Distribution Networks," in 16th Power Systems Computation Conference (PSCC 2008), Glasgow, Scotland, 2008.

[12] K. Christakou, D.-C. Tomozei, J.-Y. Le Boudec and M. Paolone, "GECN: Primary Voltage Control for Active Distribution Networks via Real-time Demand-Response," IEEE Transactions on Smart Grid, vol. 5, no. 2, pp. 662-631, 2014.

[13] B. Stott and O. Alsac, "Fast Decoupled Load Flow," IEEE Transactions on Power Apparatus and Systems, Vols. PAS-93, no. 3, pp. 859-869, 1974.

[14] R. A. Jabr and I. Džafić, "Sensitivity-Based Discrete Coordinate-Descent for Volt/VAr Control in Distribution Networks," IEEE Transactions on Power Systems, vol. 31, no. 6, pp. 4670 - 4678, 2016.

[15] Z. Zhang, L. F. Ochoa and G. Valverde, "A novel Voltage Sensitivity Approach for the Decentralized Control of DG Plants," IEEE Transactions on Power Systems, vol. 33, no. 2, pp. 1566-1576, 2018.

[16] M. Kraiczy, B. York, M. Bello, D. Montenegro, S. Akagi and M. Braun, "Coordinating Smart Inverters with Advanced Distribution Voltage Control Strategies," in IEEE Power and Energy Society General Meeting, Portland, 2018.

[17] K. Christakou, J.-Y. LeBoudec, M. Paolone and D.-C. Tomozei, "Efficient computation of Sensitivity Coefficients of Node Voltages and Line Currents in Unbalanced Radial

Electrical Distribution Networks," IEEE Transactions on Smart Grid, vol. 4, no. 2, pp. 741-750, 2013.

[18] "EPRI. (2015). Open Distribution System Simulator (OpenDSS).," [Online].

[19] J. Wang, X. Zhu, D. Mulcahy, C. McEntee, D. Lubkeman, N. Lu, N. Samaan, B. Werts and A. Kling, "A Two-Step Load Disaggregation Algorithm for Quasi-static Time-series Analysis on Actual Distribution Feeders," in IEEE Power and Energy Society General Meeting, Portland, 2018.

[20] "Residential load data collected by PECAN STREET website: https://dataport.pecanstreet.org/data/interactive," [Online].

[21] F. Xie, C. McEntee, M. Zhang and N. Lu, "An Asynchronous Real-time Co-simulation Platform for Modeling Interaction between Microgrids and Power Distribution Systems," in IEEE Power & Energy Society General Meeting, Atlanta, GA, USA, 2019.

[22] K. e. a. Ding, "A Matlab-Simulink-based PV module model and its application under conditions of nonuniform irradiance," IEEE Transactions on Energy Conversion, vol. 27, no. 4, pp. 864-872, 2012.

[23] K. Dehghanpour, Z. Wang, J. Wang, Y. Yuan and F. Bu, "A survey on state estimation techniques and challenges in smart distribution systems," IEEE Transactions on Smart Grid, vol. 10, no. 2, pp. 2312-2322, 2019.

[24] S. Weckx, R. D'Hulst and J. Driesen, "Voltage Sensitivity Analysis of a Laboratory Distribution Grid with Incomplete Data," IEEE Transactions on Smart Grid, vol. 6, no. 3, pp. 1271-1280, 2015.

[25] J. Deboever, S. Grivalja, J. Peppanen, M. Rylander and J. Smith, "Practical data-driven methods to improve the accuracy and detail of hosting capacity analysis," in IEEE 7th

World Conference on Photovoltaic Energy Conversion, Waikoloa Village, Hawaii, USA, 2018.

[26] V. Rigoni, A. Soroudi and A. Keane, "Use of fitted polynomials for the decentralised estimation of network variables in unbalanced radial LV feeders," IET Generation, Transmission & Distribution, vol. 14, no. 12, pp. 2368-2377, 2020.

[27] W. Ren and H. Ghassempouraghamolki, "Tuning of Voltage Regulator Control in Distribution," in IEEE Power and Energy Society General Meeting, Portland, OR, USA, 2018.